GEOMETRY OF CALCITE CEMENTED CONCRETIONS OF THE ARIKAREE GROUP (TERTIARY): A CLUE TO HYDRODYNAMIC PROCESSES OF CEMENTATION

BY

CHARLES EMMETT GELL, B.A.

THESIS

Presented to the Faculty of the Graduate School of

The University of Texas at Austin

in Partial Fulfillment

of the Requirements

for the Degree of

MASTER OF ARTS

THE UNIVERSITY OF TEXAS AT AUSTIN

MAY, 1996

GEOMETRY OF CALCITE CEMENTED CONCRETIONS OF THE ARIKAREE GROUP (TERTIARY): A CLUE TO HYDRODYNAMIC PROCESSES OF CEMENTATION

APPROVED BY
THESIS COMMITTEE:

Earle F. McBride

Lynton S. Land

Robert L. Folk

Dedication

To my Father for his continuous support, to my Mom for her inspiration and confidence in me, and to my girlfriend Christi Weismantel for vastly improving the quality of my life.

ACKNOWLEDGMENTS

I would like to thank Dr. Earle McBride for his patience, availability, and willingness to answer questions as well as for suggesting such an interesting project. I would also like to thank Dr. Lynton Land for his help with carbon and oxygen isotopes, Dr. Robert Folk for his help with the SEM, Rachel Eustice for her help with many aspects of this study, Dr. Leo Lynch for his clay expertise, Tor Steinke for his assistance in the field, and the Oglalla Sioux for allowing me to work on the Pine Ridge Reservation.

I would also like to acknowledge the generous financial support given to me from Gerry Malanka, Union Pacific Resources, the Geology Foundation, and the J. Nalle Gregory Chair in Sedimentary Geology.

ABSTRACT

Geometry of Calcite Cemented Concretions of the Arikaree Group (Tertiary): A Clue to Hydrodynamic Processes of Cementation,

by

Charles Emmett Gell, M.A.

The University of Texas at Austin, 1996

SUPERVISOR: Earle McBride

Eolian and fluvial deposits of the Arikaree Group (Tertiary) of western Nebraska, eastern Wyoming, and southwestern South Dakota contain abundant calcite-cemented concretions and paleosols with a variety of morphologies and distribution patterns. The morphologies include: laterally extensive horizons, highly elongate forms in the plane of bedding, rhizocretions, spheres, and sand crystals occurring as both single crystals and clusters. Calcite was precipitated from groundwater during ionic diffusion, during fluid flow in the phreatic zone, and during vadose processes. The distribution of concretions in outcrop was found to be selective to zones of coarser grain size and higher permeability for elongate forms, to areas of lower fluid flow velocity for diffusion-generated forms, and to areas which were once pedogenic horizons for concretions created by vadose processes.

Elongate "pipy" concretions, which are found as isolated, regularly spaced and laterally merging concretions, generally show a preference for particular stratigraphic

horizons, and were found to favor zones of coarser grain size and higher permeability. The orientation of the elongate concretions is remarkably uniform (the standard deviation of the axial trends are less than 14 degrees at any one locality) and parallel with the inferred regional fluid flow, which has remained unchanged since the Miocene. Rhizocretions were observed in the process of forming around modern roots. Massive laterally extensive cemented horizons are interpreted to be ancient pedogenic horizons by their abundance of burrows and bioturbation. Sand crystal rosettes are interpreted to be replacement features after gypsum rosettes. Spherical concretions and scalenohedral calcite sand crystals formed by ionic diffusion.

Electron microprobe analyses indicate that the calcite cement is close to stoichiometrically pure calcite. Oxygen and carbon isotope ratios show that the diagenetic fluid was meteoric water. Cementation occurred before significant burial. Some calcite samples were found to have a complex cement stratigraphy in cathodoluminescence, indicating episodic fluctuation in groundwater composition or temperature.

The calcite in the pipy concretions has been imported from limestone units which crop out up hydrogeologic gradient from the Arikaree. Dissolution features are present in pedogenic horizons and in some pipy concretions. Local dissolution of calcite is thought to supply calcite to vertical concretions. Fluvial channels contain clasts of pipy concretions indicating that calcite cementation occurred during deposition.

TABLE OF CONTENTS

LIST OF TABLES AND FIGURES

Table

Figure

PROJECT DESCRIPTION

Introduction

Calcite is the most abundant cement in sandstones of Mesozoic and Cenozoic age (Tallman, 1949). Unlike quartz cement, which tends to precipitate incrementally around all detrital quartz grains, ultimately filling all pores uniformly if sufficient silica is available (Pettijohn et al., 1987; McBride, 1989), calcite cement is patchy at many scales of occurrence. Although it can completely cement beds (e.g., McBride, 1978), calcite commonly forms discrete and tightly cemented bodies (concretions) embedded in weakly cemented or uncemented host sands. The ability to predict and understand the distribution of calcite-cemented sand bodies is important, because the distribution of calcite cement influences fluid flow paths of hydrocarbons and water (Kantorowicz et al., 1987; Saigal and Bjorlykke, 1987; Sharp and McBride, 1989; Bjørkum and Walderhaug, 1990).

Additionally, carbonate cement affects the quality of hydrocarbon and water reservoirs. Nodular, laterally discontinuous cemented sandstones are only likely to influence fluid flow locally, whereas laterally continuous cemented sandstone may compartmentalize reservoirs. Whether this is beneficial or detrimental depends upon the orientation of the cemented sandstone and the nature of hydrocarbon development. Thus, prediction of the geometry and distribution of carbonate-cemented concretions is desirable. Such a prediction requires an understanding of the origin of the cement and subsequent controls on its distribution (Kantorowicz, 1987).

Although calcareous concretions are a common diagenetic feature throughout the geological record, the processes controlling concretion distribution and morphology

are poorly understood. Theoretical models exist for loss of porosity from compaction (McBride, 1978; Lundegard, 1989), but there are no general theories to explain the loss of porosity from authigenic calcite cementation in terrigenous sands, which is common and widespread.

Purpose of Study

The purpose of my study is to determine the patterns, morphology, and origin of calcite-cemented concretions in the non-marine Arikaree Group (**Fig. 1**) and to create a theoretical model for their formation, distribution, and morphology. The Arikaree was chosen for a field and lab study because it has many patterns of calcite cement (sand crystals, elongate concretions in the plane of bedding, rhizocretions, laterally continuous horizons, and spheres) and the general diagenetic is known (Stanley and Benson, 1979). Whereas there have been many studies of calcite-cemented concretions in marine sands (e.g., Bjørkum and Walderhaug, 1990; Coleman, 1993), there have been relatively few studies on non-marine sands.

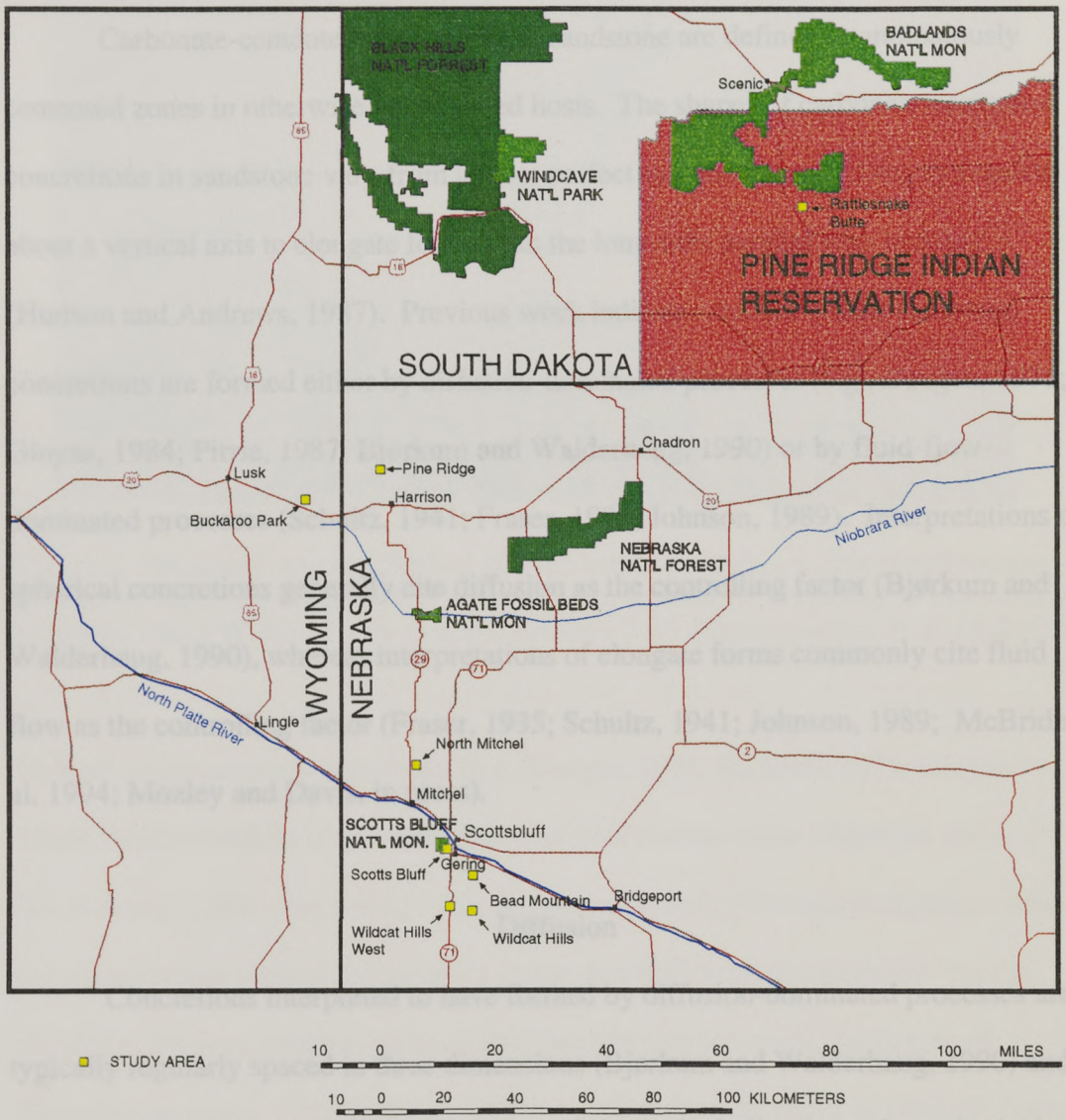

Figure 1. Extensively studied and sampled field localities are indicated by yellow boxes.

Previous Work

Summary

Carbonate-cemented concretions in sandstone are defined as anomalously cemented zones in otherwise uncemented hosts. The shapes of carbonate-cemented concretions in sandstone vary from almost perfect spheres through discs symmetric about a vertical axis to elongate forms with the long axes parallel with bedding (Hudson and Andrews, 1987). Previous work indicates that carbonate-cemented concretions are formed either by diffusion-dominated processes (e.g., Deegan, 1971; Gluyas, 1984; Pirrie, 1987; Bjørkum and Walderhaug, 1990) or by fluid-flow-dominated processes (Schultz, 1941; Fraser, 1935; Johnson, 1989). Interpretations of spherical concretions generally cite diffusion as the controlling factor (Bjørkum and Walderhaug, 1990), whereas interpretations of elongate forms commonly cite fluid flow as the controlling factor (Fraser, 1935; Schultz, 1941; Johnson, 1989; McBride et al. 1994; Mozley and Davis, in press).

Diffusion

Concretions interpreted to have formed by diffusion-dominated processes are typically regularly spaced in three dimensions (Bjørkum and Walderhaug, 1990) and spherical (**Fig. 2**), but may possess a range of shapes including irregular, spherical or oblate spheroids that are flattened in the plane of bedding (e.g., Deegan, 1971; Gluyas, 1984; Pirrie, 1987; Bjørkum and Walderhaug, 1990). Deviations from spherical shapes have been explained as a result of varying growth rates in different directions

Figure 2. Regularly spaced spherical and spheroidal concretions interpreted to have formed by diffusion-dominated processes. Intra-Apenninic Pliocene, 15 km south of Bologna, Italy. Width of view is approximately 5 m. Photo courtesy E. F. McBride.

because of permeability anisotropy (e.g., Deegan, 1971; Raiswell, 1971; Gluyas, 1984), or inhomogeneous primary distribution of marine shells (Bjørkum and Walderhaug, 1990). According to the former hypothesis, flattened concretions form in sediments where vertical permeability is less than horizontal permeability. As the difference between vertical and horizontal permeability increases, the degree of flattening increases. Spherical concretions are, therefore, the result of isotropic host fabric. Regular spacing has been explained by a lowering of dissolved calcium-bicarbonate concentrations in the adjacent pore water after nucleation, thus inhibiting nucleation of additional concretions in the surrounding area or "sphere of influence"(Bjørkum and Walderhaug, 1990).

Diffusion models include the concept that concretions grow by the diagenetic redistribution of calcium carbonate derived from fossils, limestone rock fragments, or Ca-plagioclase within a sphere of influence a meter or two in diameter around the nucleation point (Bjørkum and Walderhaug, 1990). If the source of cement is internal, the calcite need only be transported short distances from the site of dissolution to the site of precipitation. Stratabound concretions and laterally continuous cemented layers have been attributed to cementation of primary shell layers in marine sand (Davies, 1969; Kantorowicz et al., 1987; Bjørkum and Walderhaug, 1990). If the major source of dissolved calcium carbonate is marine fossils, supersaturation and nucleation points should be found preferentially in fossil-rich layers.

Bathurst (1975) and Berner (1980) were the first to show that in order to precipitate one pore volume of calcite cement by fluid flow, at least 100,000 to 300,000 pore volume exchanges of aqueous solution, need to take place. Bjørkum and Walderhaug (1990) state that the fluid volume necessary for so many pore volume exchanges is impossible to supply by normal fluid flow and that diffusion, therefore, must be the process of material transport during the cementation process. If diffusion is the dominant process, the source of calcite in shallow marine sandstone must always be derived from the local sandstone.

Fluid Flow

Concretions interpreted to have formed by fluid-flow-dominated processes form horizontal elongate concretions (**Fig. 3**) which have a locally consistent orientation of the elongate axes (Schultz, 1941; McBride et al., 1994; Mozley and Davis, in press). The distribution and morphology of these highly prolate-shaped concretions has been interpreted as selective growth in the direction of regional groundwater flow (Schultz, 1941; Fraser, 1935; Johnson, 1989), growth parallel with bedding planes (Raiswell, 1971; Deegan, 1971; Gluyas, 1984), and growth in the direction of preferred grain alignment (Pirrie, 1987). Diffusion is not the dominant process in fluid-flow models, and carbonate cement may be derived from distances much greater than the 1-2 m sphere of influence around the nucleation point proposed in Bjørkum and Walderhaug's (1990) diffusion model. Importing calcite from outside a 1-2 m sphere in reasonable geologic time can only be accomplished through groundwater flow.

Cylindrical concretions with a pattern of horizontal elongation have been noted in many studies (Todd, 1903; Schultz, 1941; Meschter, 1958; Colton, 1967; Jacob, 1973; Raiswell and White, 1978; Parsons, 1980; Theakstone, 1981; Fastovsky and Dott, 1986; Pirrie, 1987; Johnson, 1989; McBride et al., 1994; Mozley and Davis, in press). Fraser (1935), Schultz (1941), and Mozley and Davis (in press) interpreted horizontally elongate cylindrical concretion morphologies as a function of fluid flow within the host sandstone. They believed that more permeable lenses channeled meteoric fluid such that sandstone was preferentially cemented where fluid flow was greatest.

Figure 3. Elongate concretions parallel with bedding interpreted to have formed by fluid-flow dominated processes. Monroe Creek-Harrison formations, Bead Mountain, Nebraska.

In the calcite-concretions of the Arikaree Group, most of the concretions have locally parallel axial trends (Schultz, 1941). Between localities, however, variations in orientation of as much as 20 degrees may exist. These variations are explained by Schultz as reflecting local basement highs which diverted groundwater flow paths around them. Schultz also observed that the concretions encircle uplifted areas, and hypothesized that structures such as anticlines may be mapped by utilizing the trends of concretions.

Causes of Carbonate Precipitation

Calcite will precipitate when the activity of Ca^{++} and $CO^{=}_{3}$ are raised above the solubility product as when CO_2 is outgassed from pore fluids. Conditions proposed to accomplish this include: 1) an increase in temperature in descending pore fluids (calcite solubility decreases with increasing temperature), 2) decrease in pCO_2 in ascending pore fluids (Lundegard and Land, 1986), 3) mixing two different pore fluids in equilibrium with calcite (Drever, 1988), 4) dissolution of metastable aragonite or Mg-calcite skeletal grains and carbonate rock fragments in sandstone (Kantorowicz et al., 1987), 5) pressure solution of carbonate grains in sandstones or in deeper-buried carbonate rocks, 6) increase in alkalinity associated with an increase in the rate of Fe reduction (Curtis and Coleman, 1986), 7) increase in alkalinity associated with the decay of organic tissue and the generation of ammonia, 8) decrease in acidity in the microenvironment where H^+ are adsorbed onto mica surfaces (Boles and Johnson, 1983), and 9) increase in alkalinity resulting from release of CO_2 from organic matter and methane through bacterially mediated redox reactions (Hoveland et al., 1985; Curtis and Coleman, 1986).

Carbon and Oxygen Isotopes

The dissolution and reprecipitation mechanisms of $CaCO_3$ are particularly important to the investigation of the evolution of concretions, because they may leave distinctive $^{12}C/^{13}C$ and $^{16}O/^{18}O$ signatures. Carbonates that precipitated from CO_2 derived from organic material commonly have lighter carbon isotopic compositions than carbonates precipitated from groundwater or from the ocean. Systematic variation

in the isotopic composition of carbon can yield valuable data regarding the fluid history during concretion growth (e.g. Bjørkum and Walderhaug, 1993).

$\delta^{18}O$ of carbonate is controlled by two parameters: the oxygen isotopic composition of the pore-waters and the temperature at the time of precipitation. In authigenic calcite, it can be difficult to separate the influence of each parameter. However, where there is a clear sequence of intergranular diagenetic cements, there is commonly a decrease in $\delta^{18}O$ values with increased burial depth. This is primarily the effect of increased temperature. If this relationship is present, this isotopic variation can be used to better understand the factors controlling concretion geometry by mapping variations in a particular concretion and observing systematic variations around its nucleation point.

Several authors have suggested that calcite-cemented layers in sandstone may form by merging concretions (Berner, 1980; Fürsich, 1982; Bryant et al., 1988; Bjørkum and Walderhaug, 1990). If this hypothesis is correct, a systematic variation of $\delta^{18}O$ values from the nucleation points to the margins of concretions may be present, assuming that no major shifts in oxygen isotopic composition of the pore water took place during calcite precipitation other than that caused by increases in temperature with time. Concretion centers (nucleation points) should have the least negative values and the latest precipitated infill of calcite cement should have the most negative $\delta^{18}O$ values. Although several authors have presented $\delta^{18}O$ values of calcite cement measured at closely spaced locations across concretions in shales (Coleman and Raiswell, 1981; Coniglio and Cameron, 1990), few data have been published on the detailed $\delta^{18}O$ patterns in sandstones (Wilkinson, 1991).

Bjørkum and Walderhaug (1993) measured $\delta^{18}O$ and $\delta^{13}C$ values for calcite cement in a two dimensional vertical grid located within a laterally extensive calcite-cemented layer in the Lower Jurassic Birdport Sands, southern England, in order to determine whether the isotopic data indicate that the layer formed from merging concretions. The result of the study indicate that calcite cement nucleated at points with lateral spacing of 0.5 to 1 m. The $\delta^{18}O$ values decreased from probable nucleation points, suggesting that calcite-cement grew outward from these nucleation points as individual concretions increased in size until they merged to form a continuous layer. A similar approach by Milliken et al. (in review) for shallow marine Pliocene sandstones in Italy yielded negative results. No concretion nuclei could be identified.

Regional Geology

The Cenozoic strata of western Nebraska, west central Wyoming, and south western South Dakota are composed of extensive sequences of continental deposits that extend eastward from the Hartville, Laramie, and Front Range uplifts and southeast from the Black Hills (Wanless, 1922; 1923; Sato and Denson, 1967; Stanley, 1976). East of the Laramie Range, the High Plains sequence consists of a wedge of Oligocene through Pliocene fluvial, eolian, and lacustrine rocks that extends several hundred kilometers from the mountain front (Stanley and Benson, 1979).

In eastern Wyoming and adjoining Nebraska, these rocks rest unconformably on gently folded Cretaceous rocks, and locally, on a late Eocene lateritic paleosol developed on Cretaceous rocks (Pettyjohn, 1966). Stratigraphic evidence indicates that the relationship between the sedimentary basin of the High Plains sequence to adjacent

uplifts has not changed greatly either physiographically or structurally since the onset of continental sedimentation during the earliest Oligocene (Denson and Bergendahl, 1961; Clark et al., 1967; Stanley, 1971).

The oldest Cenozoic sediments (Chadron Formation, White River Group) are early Oligocene alluvial valley fills. Subsequent to filling these drainages and continuing for about the next 7 m.y., landscape development in the area was dominated by eolian deposition of tremendous volumes of rhyolitic volcanic ash derived from western eruptions. A plain of low relief, with only narrow local drainages was maintained during most of this period (Stanley and Benson, 1979).

Uplift in the Rocky Mountains and Great Plains (pre-Gering Formation, Arikaree Group) caused widespread fluvial erosion and brought epiclastic detritus into the area about 28 m.y. ago. This erosion produced the unconformity which separates the Gering Formation (Arikaree Group) from older Cenozoic units. The principle differences between the pyroclastic materials in the Arikaree Group and those of the older White River Group are the coarser grain size and smaller percentage of glass shards in the Arikaree. The total pyroclastic contribution to the eolian deposits of the Arikaree Group, however, still approaches 75% (Vicars and Breyer, 1981; Hunt, 1981)

A second period of regional erosion, typified by valleys of low relief and low-angle side slopes, resulted in an unconformity that separates Monroe Creek-Harrison sediments from the Upper Harrison beds. Following the filling of these valleys, the accumulation of pyroclastic material once again resumed and eolian deposits of the Upper Harrison blanketed much of the area. Eolian sediment consisting mostly of pyroclastic detritus continued building the plains during and after Gering alluvial

deposition until about 19 m.y. ago when Arikaree deposition ceased. About this time, western volcanic activity declined for several million years and was followed by a marked decrease in the volume of rhyolitic volcanism for the remainder of the Cenozoic (Swinehart et al., 1985).

Stratigraphy

The stratigraphy of the Arikaree Group has been the subject of controversy since the 1930's (see discussions by McKenna, 1965; Skinner et al., 1977; Hunt, 1981). Based on lithologic and mineralogic similarities, biostratigraphy, and E-log characteristics, Swinehart et al. (1985) divided the Arikaree Group into three units (**Fig. 4**): 1) the Gering Formation; 2) Monroe Creek-Harrison formations; and 3) the Upper Harrison beds. In the northeast, the Arikaree Group is generally browner and finer grained, making it so lithologically similar to the White River Group that it is difficult to differentiate (Swinehart et al., 1985).

The Gering Formation has a maximum thickness of 107 m and is generally finer grained northeastward. It is lithologically characterized as orange-gray, massive, medium-grained volcaniclastic sandstone to siltstone, which weathers into vertical cliffs and columnar-type badlands. Calcite-cemented concretions are present in irregularly spaced layers throughout the unit, either as individual "pipes" or coalesced into laterally extensive ledges. Small hard nodular concretions 7 to 12 cm in diameter occur locally

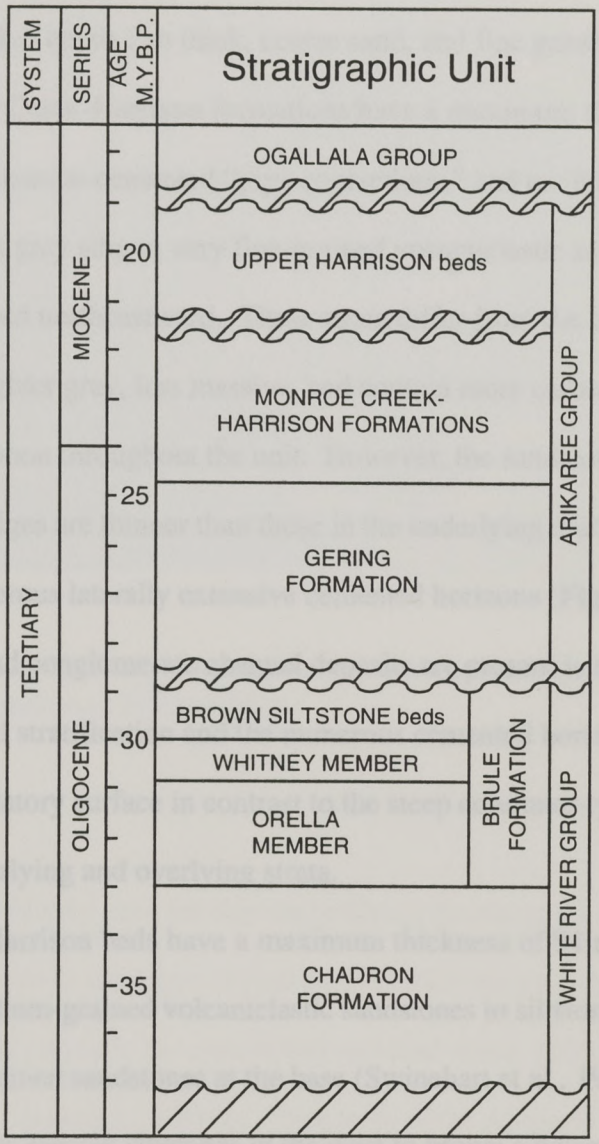

Figure 4. Idealized time stratigraphic section of the Arikaree Group showing unconformities. From Swinehart et al. 1985.

in the lower part of the unit. In some areas, poikilotopic calcite has formed around sand grains, resulting in calcite sand crystals. The Gering formation includes locally occurring beds of ash 5 cm to 1 m thick, coarse sand, and fine gravel.

The Monroe Creek-Harrison formations have a maximum thickness of 128 m, contain abundant carbonate-cemented "pipy concretions," and are lithologically characterized as light gray silty to very fine-grained volcaniclastic sandstones, which are generally finer-grained northeastward. These strata differ from the beds below in that they are generally lighter gray, less massive, and contain more carbonate cement. Pipy concretions are common throughout the unit. However, the sandstone layers between the concretionary ledges are thinner than those in the underlying unit. Bedding is accentuated by numerous laterally extensive cemented horizons (**Fig. 5**). Coarse-grained sandstone and conglomerate channel deposits are present locally. Because of the more pronounced stratification and the numerous cemented horizons, this unit weathers to an undulatory surface in contrast to the steep columnar-type badlands common in the underlying and overlying strata.

The Upper Harrison beds have a maximum thickness of 91 m and are characterized as medium-grained volcaniclastic sandstones to siltstones with locally occurring coarser-grained sandstones at the base (Swinehart et al., 1985). The unit generally grades from grayish siltstones in the west to brown siltstone to fine-grained sandstone in the northeast and contain abundant silicified root casts (McGrew, 1963). Thin claystone and tuff beds are locally interbedded with the sandstone. Thick sandstone beds between calacareous concretionary ledges weather into vertical cliffs and columnar-type badlands.

Figure 5. Laterally extensive cemented horizons accentuating bedding in the Monroe Creek-Harrison formations at Wildcat Hills.

METHODS

I collected field data used for this study during the summers of 1994 and 1995. My goal in the field was to catalogue as many geometries and patterns of calcite cement as possible, extensively sample the concretions and host sands, and to determine the distribution of calcite cement in outcrop. Exposures of the Arikaree were found throughout the panhandle of western Nebraska, south western South Dakota, and eastern Wyoming with the aid of a regional geologic map, previous studies, several paleontological guidebooks, and extensive driving. Localities which contained previously uncataloged concretion geometries or stratigraphic relationships were

studied more extensively (**Fig. 1**). At these localities, I photographed concretions, described them in outcrop, recorded the axial trends of elongate concretions with a Brunton compass, and took samples of the concretions and adjacent uncemented host sands. The most intensely studied localities are in the Wildcat Hills and Pine Ridge escarpments in Nebraska and Rattlesnake Butte in South Dakota.

75 standard thin sections were made of laterally extensive horizons, highly elongate concretions in the plane of bedding, rhizocretions, spheres, scalenohedral sand crystals, and gypsum pseudomorphs, as well as uncemented host sands adjacent to these cemented forms. All were vacuum impregnated with blue-dyed epoxy resin before being thin sectioned. Petrographic data (mineral composition and texture) were obtained by point-counting 300 points in 30 samples. Grain-size analysis was performed on 30 thin sections by measuring the long axis of 50 grains per thin section. Attempts to stain for K-feldspar were unsuccessful. Thin sections were etched in HF vapor for 10 seconds to enhance cleavage in untwinned feldspar grains, making differentiation from quartz easier. 15 polished thin sections were made for analysis by cathodoluminescence (CL) and electron probe microanalysis (EPMA).

Scanning electron microscopy (SEM) was used on 24 samples to help determine the relative timing of diagenetic events, identify and characterize the distribution of authigenic clay coats, and to characterize the detrital grains. An X-ray analyzer (EDS) attached to the SEM was used for qualitative analysis to aid in grain identification.

Analysis of clay components was achieved by XRD. 10 samples were disaggregated ultrasonically in the presence of a dispersant. The $< 2\mu$ fraction was

removed by centrifuge and saturated with ethylene glycol. Air dried and glycol solvated XRD spectra were collected on a Siemens D-500 diffractometer using Cu radiation, 0.02 degree 2 theta step size and a two second count time. A comparison of the patterns before and after saturation indicated the presence of smectite.

Conventional cathodoluminescence (CL) was used on 15 polished thin sections to investigate the cementation history and trace element distribution of calcite cement.

WDS analyses were performed on 3 polished thin sections of a pipy concretion, a sample from a pedogenic horizon, and a gypsum pseudomorph using a JEOL 733 supermicroprobe with a 12 μ spot and a 10 nA sample current. Analyzed elements and count times were Ca (10 sec.), Mg (40 sec.), Sr (60 sec.), Fe (60 sec.), and Mn (40 sec.).

$\delta^{13}C$ and $\delta^{18}O$ were determined on 40 calcite samples. The analytical procedures and fractionation factors used are from Land (1984).

PETROGRAPHY AND PROVENANCE

Framework

Quartz

Quartz framework grains include grains with straight extinction, undulose extinction and composite varieties. Blatt and Christie (1963) noted that volcanic extrusive quartz is characterized by high proportions of straight extinction quartz, whereas composite and undulatory grains are usually associated with igneous and metamorphic sources. The Arikaree Group contains more quartz grains with

composite and undulose extinction, whereas euhedral volcanic quartz grains were not observed. This may reflect the proximity of the plutonic and metamorphic rocks of the Laramie Range.

Feldspars

All feldspar grains were lumped into one category due to the difficulty of differentiating potassium feldspar from plagioclase. 75 percent of the feldspar grains present are untwinned. The primary feature used to differentiate feldspar from quartz was identifying the presence of cleavage which was accentuated by etching in HF fumes. Feldspar grains present in the Arikaree Group include orthoclase, microcline, and plagioclase.

Volcanic Rock Fragments and Shards

Pyroclastic detritus was not differentiated and includes volcanic glass shards, pumice fragments, and volcanic rock fragments (**Fig. 6**). Volcanic glass shards include all angular volcanic glass fragments which do not contain vesicles. Pumice fragments are characterized as extremely vesicular fragments, which tend to be less angular than shards. Volcanic rock fragments are characterized as rock fragments which contain volcanic glass but are not shards or pumice. Most pyroclastic detritus is preserved as fresh glass with little alteration and no zeolitization.

Miscellaneous Minerals

Nonopaque heavy mineral components are similar to those found by Sato and Denson (1968), Denson (1969), Denson and Chisholm (1971), and Bart (1974). The majority of heavy minerals present are of volcanic origin and include green-brown hornblende and augite. Less than 25 percent of the heavy minerals present are plutonic in origin and include tourmaline, garnet, and staurolite. Muscovite, biotite, and fragments of mica schist are present locally. Opaque heavy minerals compose less than 1 percent of the framework grains present and include magnetite, ilmenite (Bart, 1974), and hematite-coated olivine grains.

General Features

Detrital mineralogy indicates that the Arikaree Group is mineralogically immature with a large proportion of chemically unstable framework constituents. Carbonate rock fragments were only found locally at Rattlesnake Butte and are not believed to be a potential cement source. Sandstones are classified as feldspathic and vitric litharenites (after Folk, 1968) (**Fig. 7**). Grains are angular to sub-angular and well sorted. Average grain size is 3.2ϕ for calcite-cemented sands and 3.4ϕ for uncemented sands (**Fig. 8**).

Figure 6. Photomicrograph of a typical uncemented sample showing a variety of shard and pumice grains. Field of view is 1.7 mm wide. Bead Mountain, Arikaree Group.

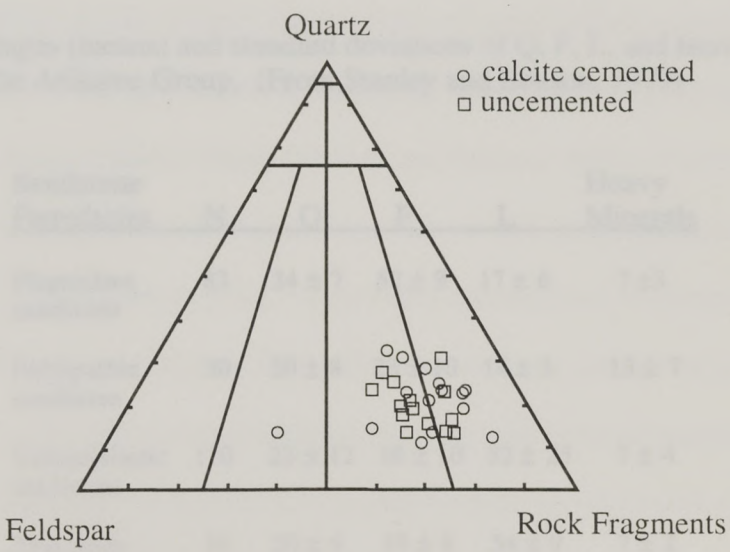

Figure 7. Sandstones in the Arikaree Group are classified as vitric and feldspathic litharenites (after Folk, 1968).

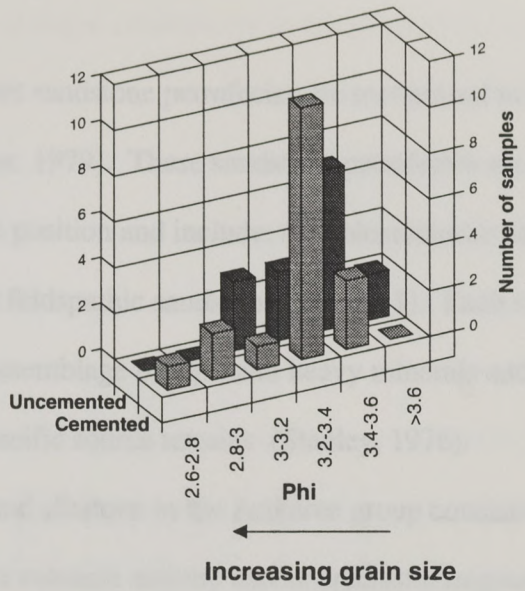

Figure 8. Grain size distribution of cemented and uncemented sands from the Arikaree Group.

Table 1. Averages (means) and standard deviations of Q, F, L, and heavy minerals for sandstone in the Arikaree Group. (From Stanley and Benson, 1979)

Sandstone Petrofacies	N	Q	F	L	Heavy Minerals
Plagioclase sandstone	83	24 ± 7	52 ± 9	17 ± 6	7 ±3
Feldspathic sandstone	30	50 ± 8	23 ± 10	14 ± 5	13 ± 7
Volcaniclastic sandstone	110	23 ± 12	18 ± 10	52 ± 25	7 ± 4
This study	30	20 ± 6	19 ± 8	54 ± 9	7 ± 2

N is the number of thin sections counted. Values for quartz (Q), Feldspar (F), lithic and granitic fragments (L), and heavy minerals are volumetric percentages of the total framework.

Provenance

Three distinct sandstone petrofacies are recognized in the Arikaree Group (Stanley and Benson, 1979). These sandstone petrofacies are independent of grain-size and biostratigraphic position and include: (1) volcaniclastic sandstones, (2) plagioclase sandstones, and (3) feldspathic sandstones (**Table 1**). Each sandstone petrofacies contains a unique assemblage of light and heavy minerals and lithic fragments, which can be related to specific source terrains (Stanley, 1976).

Sandstone and siltstone in the Arikaree group consists of pyroclastic detritus derived from distant volcanic activity and of epiclastic fragments eroded from Precambrian crystalline rocks, Paleozoic and Mesozoic sedimentary rocks, and Cenozoic volcanic rocks exposed in the Laramie and Front Ranges, Hartville uplift, and Black Hills (Wanless, 1922; 1923; Sato and Denson, 1967; Stanley, 1976).

East of the Laramie Range, volcaniclastic rocks are siltstone, mudrock, and very fine-grained to fine-grained vitric litharenite, which together comprise the main body of rocks of the Arikaree Group (Stanley and Benson, 1979). These rocks contain 40 to 80 percent rhyolitic volcanic glass fragments, which include shards and pumice grains (**Fig. 6**). Pyroclastic material was probably ejected from volcanoes west of the High Plains (Stanley and Benson, 1979). The volcaniclastic sandstone petrofacies of the High Plains and in the intermontane basins to the west were deposited contemporaneously with an episode of immense volcanic activity in the eastern Great Basin of Nevada and Utah (Armstrong, 1968). The latter area is the most likely source of the rhyolitic glass in sandstone and ash beds of the Arikaree Group (Stanley and Benson, 1979).

The source of major constituents in the plagioclase sandstone petrofacies is the Laramie anorthosite complex in the central Laramie Range where norite, anorthosite, and hypersthene syenite are the dominate lithologies (Stanley, 1976). Minerals and lithic fragments that make up the feldspathic sandstone petrofacies, however, are comparable to minerals in granitic and metamorphic rocks in the Hartville uplift and in the Laramie and Front Ranges (Stanley and Benson, 1979). Source rocks range from quartz syenite to granodiorite and include the Sherman batholith south of the Laramie anorthosite complex and metamorphic rocks of amphibolite facies, principally hornblende gneiss and schist, biotite, gneiss, and quartz-feldspathic gneiss (Denson and Botinelly, 1949; Osterwald and Dean, 1957; Smithson and Hodge, 1972).

Matrix

The matrix consists of interstitial smectite (identified by XRD), which constitutes as much as 10 percent of some friable sandstones, but usually is less than 3 percent. Some of this clay could have been deposited with the sand or mechanically infiltered soon after deposition, however, the box-work fabric of the smectite is typical of authigenic smectite (Wilson and Pittman, 1977) (**Fig. 9**).

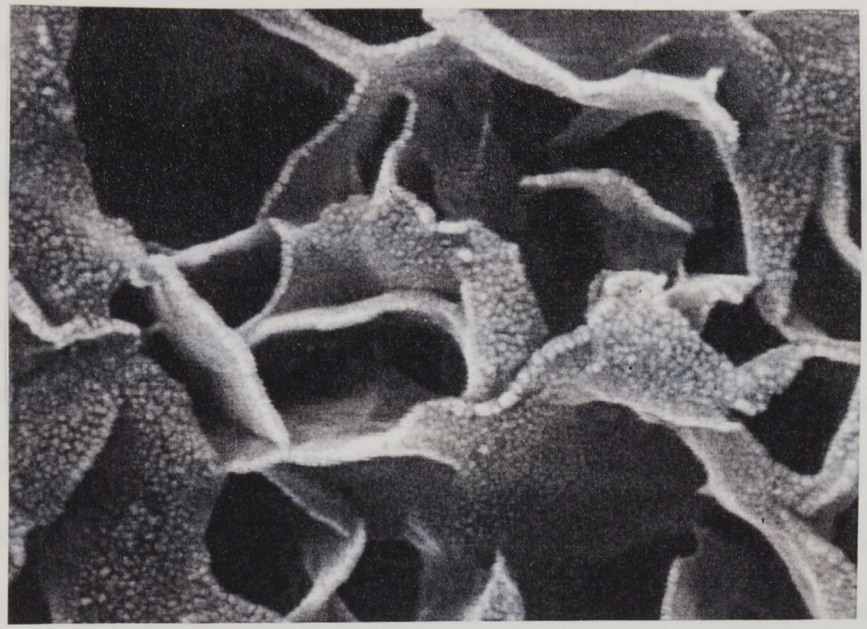

0.5 μm

Figure 9. Smectite grain coating. Bead Mountain, Arikaree Group.

Cement

Sandstone, siltstone, and volcanic ash of the Arikaree Group are cemented by calcite, smectite, and opal. Opal cement is not described here because it was only observed at the Agate Fossil Beds National Monument and has been previously described by Stanley and Benson (1979). Calcite cement occurs in 15 to 25 percent of the total rock volume in the Arikaree Group. Calcite textures include spar, poikilotopic scalenohedral sand crystals 1 to 20 cm in length, displacive sparry and micritic caliche nodules in paleosols, and as micrite forming rhizocretions and a variety of elongate

concretions in the plane of bedding. Calcite was found throughout the Arikaree Group in sandstone, siltstone and ash horizons.

Over 250 microprobe analyses were performed on calcite cement in three polished thin sections for magnesium, calcium, strontium, iron, and manganese. Of these analyses only 18 were above detection limits for elements other than calcium and of these, 15 were for magnesium and 3 for manganese. The analyses that are above detection limits are not evenly distributed on a single sample, but are spread throughout all the samples. This indicates that the calcite cement is not homogeneous with respect to trace element distribution. The results of the microprobe analyses indicate that while magnesium and manganese are not homogeneously distributed within calcite cement, the detectable concentrations are so small that they are just above detection limits and therefore the calcite is very close to stoichiometric composition.

ICP analyses were performed on 8 samples for magnesium, calcium, strontium, iron, and manganese. These analyses indicate small amounts of trace elements that were not detectable in the probe. The trace element concentrations are very low and indicate that calcite is close to stoichiometric composition.

Cathodoluminescence was performed on 15 polished thin sections from elongate forms in the plane of bedding, gypsum pseudomorphs, rhizocretions, pedogenic horizons, scalenohedral sand crystals, and spheres. Luminescence occurred in several samples. However, gypsum pseudomorphs are the only kind of concretion with consistent luminescence. The luminescence pattern shows alternating bands of luminescing and non-luminescing cement, which suggests episodic variations in the chemistry or temperature of the cementing fluid. The absence of consistent

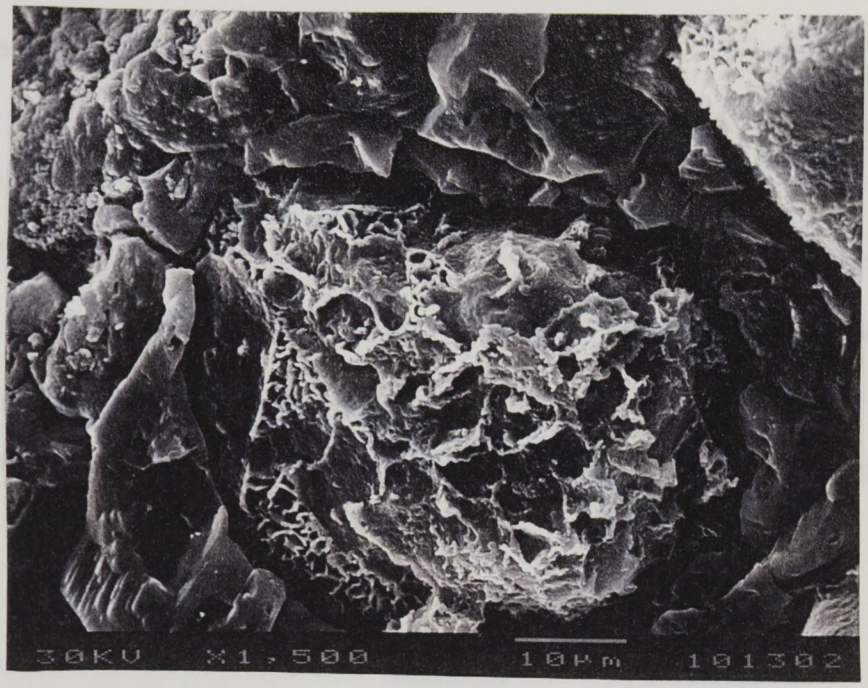

Figure 10. Smectite grain coats precipitated before calcite cement. Bead Mountain, Arikaree Group.

luminescence patterns in the majority of calcite cement indicates that iron and manganese concentrations are too low to cause luminescence.

Authigenic smectite (identified by XRD) is present locally as grain coats or highly microporous pore-fill cement in sandstones and siltstones. Grains with complete grain coats suggests that the clay precipitated at a relatively early stage of diagenesis. Where calcite and smectite are both present, smectite precipitated before calcite (**Fig. 10**). High average preserved pre-cement porosity of 45 percent (average determined by point counts) indicates that all cements precipitated soon after

deposition. A search for bacterial bodies in smectite and calcite was inconclusive and their role with respect to cement precipitation is unknown.

Porosity

The average (thin section) porosity of the uncemented and smectite cemented sands of the Arikaree Group is 37 percent. The average porosity of the calcite cemented sands is 2 percent. Minor porosity enhancement by dissolution of chemically unstable grains is present but does not contribute significantly to porosity.

Fabric

Summary

Walker stated (1967, 1976) that fabrics of continental sands are generally extensively altered during early diagenesis. The fabric of the Arikaree Group, however, shows only minor stratigraphic variations, and modifications of the original depositional fabric are restricted to modification by pedogenesis and bioturbation, inter-granular volume expansion due to the presence of displacive caliche, porosity reduction by cementation, minor porosity enhancement by dissolution of chemically unstable grains, and bending of some mica grains at grain-to-grain contacts.

Grain orientation

Laminations are visible in only a few hand specimens but are not visible in thin section. Elongate framework grains show preferential orientation in only 10 percent of samples. Bioturbation by both animals and plants and shrink-swell phenomena of

pedogenesis are thought to be responsible for this lack of primary sedimentary structure and grain orientation. Bioturbation and pedogenesis are indicated by the presence of meniscus burrow-fill textures, root traces in thin section, and the presence of abundant rhizocretions, burrows, and paleosol horizons in outcrop.

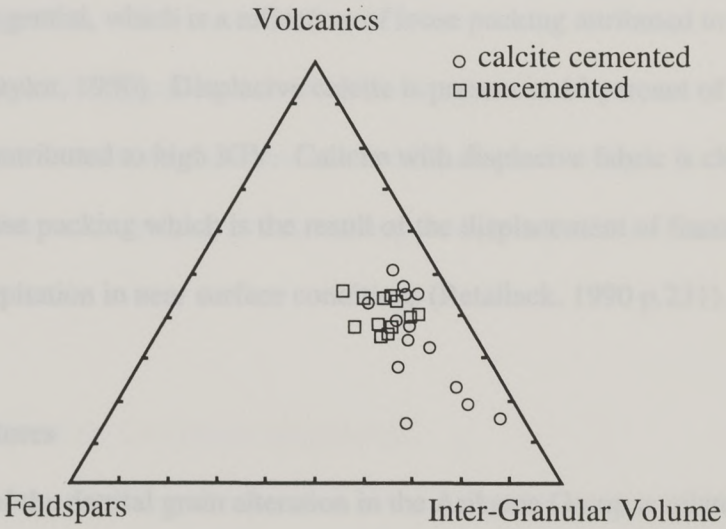

Figure 11. Ternary diagram comparing major framework grains and inter-granular volume of cemented samples and adjacent uncemented host sands from rhizocretions, gypsum pseudomorphs, elongate concretions in the plane of bedding, and pedogenic horizons. Preferential cementation of sands with higher IGV by calcite is inferred from the diagram.

Inter-Granular Volume

Point counts show that cemented samples have a high average IGV of 45 percent (**Fig. 11**), which I interpret as a reflection of depositional packing, a lack of compaction, and the local presence of displacive caliche. The irregular angular and elongate shape of many of the framework grains may have contributed to high IGV at the time of deposition. Only mica framework grains are bent and grain-to-grain contacts are tangential, which is a reflection of loose packing attributed to lack of compaction (Taylor, 1950). Displacive calcite is present in 10 percent of the samples and has also contributed to high IGV. Caliche with displacive fabric is characterized by abnormally loose packing which is the result of the displacement of framework grains by calcite precipitation in near surface conditions (Retallack, 1990 p.231).

Pedogenic Features

Much of the detrital grain alteration in the Arikaree Group is related to intrastratal solution and weathering associated with paleosol formation during the middle Tertiary (Stanley and Benson, 1979). Weathering resulted in the formation of paleosol horizons which are identified by the presence of displacive caliche, root traces, rhizocretions, evidence of intense bioturbation, and a relatively high percentage of matrix. Based on the descriptions of pedogenic horizons by Retallack (1990, p. 9-20), these paleosols are classified as aridisols with petrocalcic horizons.

Soil horizons display variable alteration of detrital grains. In calcified sand, petrocalcic horizons and surfaces of weathering, detrital grains exhibit the greatest alteration. Caliche and root horizons show replacement of feldspar by calcite (Stanley

and Benson, 1979), root casts filled with smectite, alteration of glass to smectite, and variable amounts of alteration of heavy minerals. Intrastratal solution, or the post-depositional dissolution of grains, is more uniformly distributed than soil formation and is responsible for the dissolution and partial alteration of some chemically unstable heavy mineral grains such as olivine and hypersthene. Unstable grains are less effected by intrastratal solution where they are calcite-cemented, indicating relatively early cementation by calcite.

Of the lithic fragments in the Arikaree Group, only vitric pyroclastic material shows evidence of identifiable alteration, including the development of minor secondary porosity, rounding of grains, etching, and pitting. Glass shards are commonly unaltered.

Influence of Texture on Concretion Distribution

Comparisons between the fabric of elongate concretions parallel with bedding, rhizocretions, and laterally extensive horizons and their immediately adjacent host rocks were made by point counts. A ternary diagram with porosity and diagenetic calcite on the same pole suggests that samples with higher IGV were preferentially cemented by calcite (**Fig. 11).** Some of this IGV may be due to the displacive action of caliche. However, a comparison of grain size between cemented and uncemented samples indicates that cemented samples have a coarser average grain size (**Fig. 8**). These data suggest that elongate calcite cemented concretions parallel to bedding, rhizocretions, and pedogenic horizons preferentially cements zones of higher pre-cement porosity and coarser grain size

Table 2. Summary of calcite cement morphologies and inferred growth mechanisms.

Type of Concretion	Fabric	IGV %	δ18O (SMOW)	δ13C (PDB)	Number of Samples Analysed	Inferred Growth Mechanism
Pipy	Structureless, Laminated, and Crossbedded	40.5	-10.8	-6.8	13	Fluid Flow in Phreatic Zone
Gypsum Pseudomorph	Structureless	45.3	-9.5	-6.6	2	Ionic Diffusion
Rhizocretion	Structureless	38.4	-9.9	-7.2	2	Surficial Vadose Processes
Pedogenic Horizon	Meniscus Burrow Fill	54.0	-10	-6.8	4	Surficial Vadose Processes
Scalenohedral Sand Crystals and Spheres	Undisturbed, Laminated	37.0	-12.7	-8.7	14	Ionic Diffusion
Uncemcented Host Sand	Structureless, Laminated, and Crossbedded	36.9				

GEOMETRY AND PATTERNS OF CALCITE CEMENT

General Comments

The shapes of calcite-cemented concretions observed in this study include spheres, oblate spheroids, prolate forms with various degrees of elongation oriented parallel to bedding, rhizocretions, poikilotopic scalenohedral sand crystals, and gypsum pseudomorphs. Calcite-cemented forms make up between 15 to 25 percent of the total rock volume in the Arikaree Group. Concretions are dispersed both randomly and with uniform spacing.

From previous work, I have classified concretions based on the inferred mechanisms of formation (**Table 2**). Forms elongate in the plane of bedding are interpreted to have formed through supply of calcium and bicarbonate by means of fluid flow in the phreatic zone. Spherical forms and poikilotopic scalenohedral sand crystals are interpreted to have formed by precipitation from phreatic groundwater through supply of calcium and bicarbonate by ionic diffusion. Pedogenic horizons, rhizocretions, and discontinuous lenses of gypsum pseudomorphs are interpreted to have formed through surficial vadose processes.

Forms Generated by Surficial Vadose Processes

Paleosols

Laterally continuous cemented paleosol horizons are common throughout the Arikaree Group (**Fig. 12**) and make up 10 to 20 percent of the calcite-cemented rocks. They maintain a uniform thickness which ranges from 0.5 - 1.5 m. Within the cemented horizon, calcite cement exceeds 45 percent by volume of the rock. The

horizons are characterized by the presence of discrete burrows with highly variable orientations, shapes, and sizes ranging from 1 mm to 10 cm in diameter and 1 cm to 3 m long, abundant displacive caliche nodules 1 mm to 1 cm in diameter composed of sparry calcite crystals 0.1 to 1 mm long and micritic rhizocretions containing silicified organic plant matter oriented perpendicular to the top of the soil horizon 1 mm to 1 cm in diameter and 5 to 10 cm long, organic grain coats (organans), and matrix composing 1 to 2 percent of the horizons. Based on the descriptions of pedogenic horizons by Retallack (1990, p. 9-20), I interpret these concretions to be pedogenic aridisols. Such paleosols generally take 10^3 to 10^4 years to form (Retallack, 1990 p.263).

Figure 12. Laterally continuous cemented horizon interpreted as a paleosol from North Mitchel.

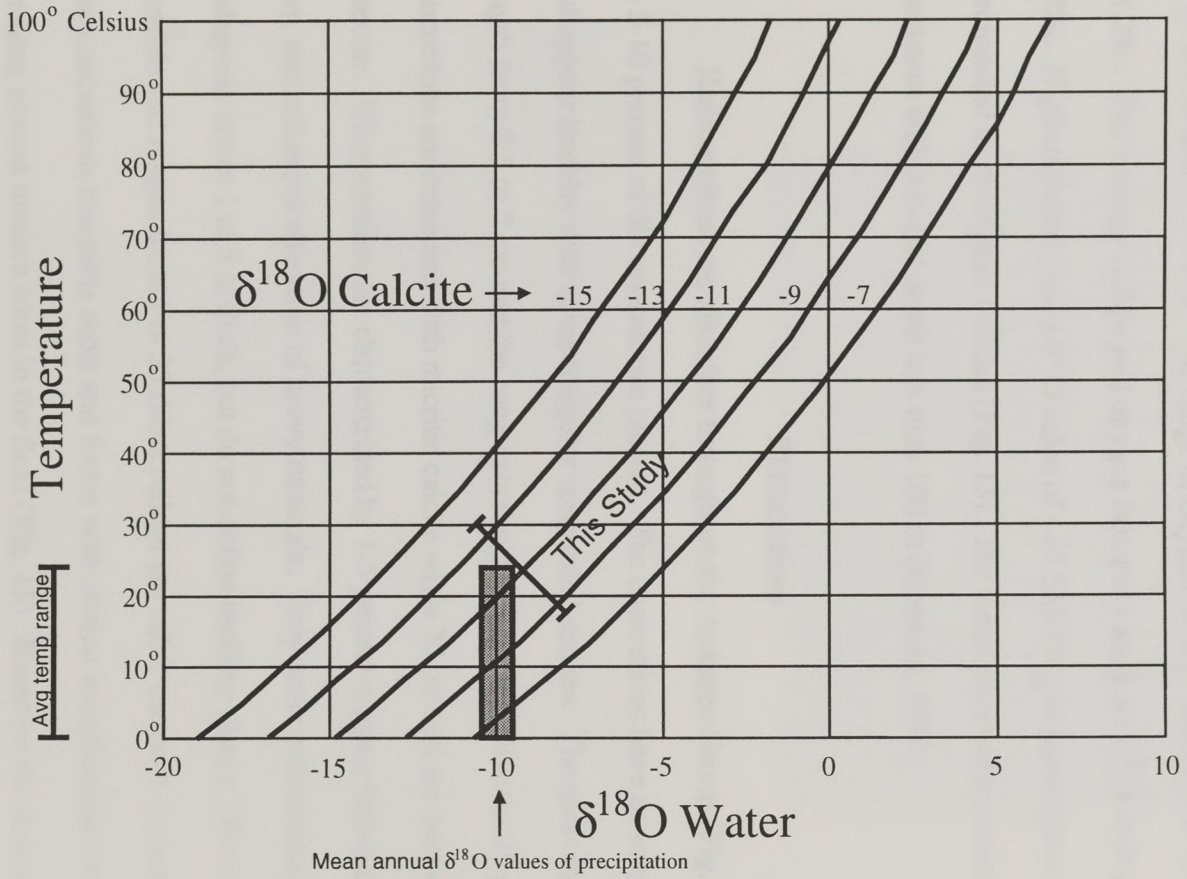

Figure 13. Graph showing the relationship between oxygen isotopes and temperature of calcite precipitation given the oxygen isotope ratio of local meteoric water.

These horizons are characterized by abnormally loose packing due to displacement by micritic and sparry caliche nodules, meniscus burrow fill textures, and enhanced alteration of heavy mineral grains. The range of carbon isotope values is $\delta^{13}C$ -6.1‰ to $\delta^{13}C$ -7.1‰. The range of oxygen isotope values is $\delta^{18}O$ -8.5‰ to $\delta^{18}O$ -11.2‰. The average carbon and oxygen isotopic values are $\delta^{18}O$ -10‰ and $\delta^{13}C$ -6.8‰. If groundwater had a $\delta^{18}O$ value of - 10 SMOW, then pedogenic calcite precipitated at 15 degrees Celsius (**Fig. 13**). The temperature of precipitation is consistent with a burial depth less than 100 m (Gosnold, 1990).

Rhizocretions

Rhizocretions are abundant throughout the Arikaree Group (**Fig. 14**) and make up 5-10 percent of the concretions present. The concretions have an irregular thickness and appear knobby with some irregular spheroidal masses. The short axis ranges in length from 0.5 to 7 cm and the long axis ranges from 10 to 40 cm. 25 percent of the concretions are cemented with micritic calcite while 75 percent are cemented with smectite. Rhizocretions are characterized by 1-5 percent organic material, infiltered clay, and enhanced alteration of heavy minerals. They occur preferentially in discrete pedogenic zones 1 to 5 m thick, but do not define bedding planes. The density is variable and ranges from 1 to 35 rhizocretions per cubic meter of uncemented host. The concretions resemble roots and forms with similar morphologies were observed forming around modern roots in the field (**Fig. 15**). Based on the descriptions of rhizocretions (Retallack, 1990 p.26), I interpret these concretions to have formed around roots.

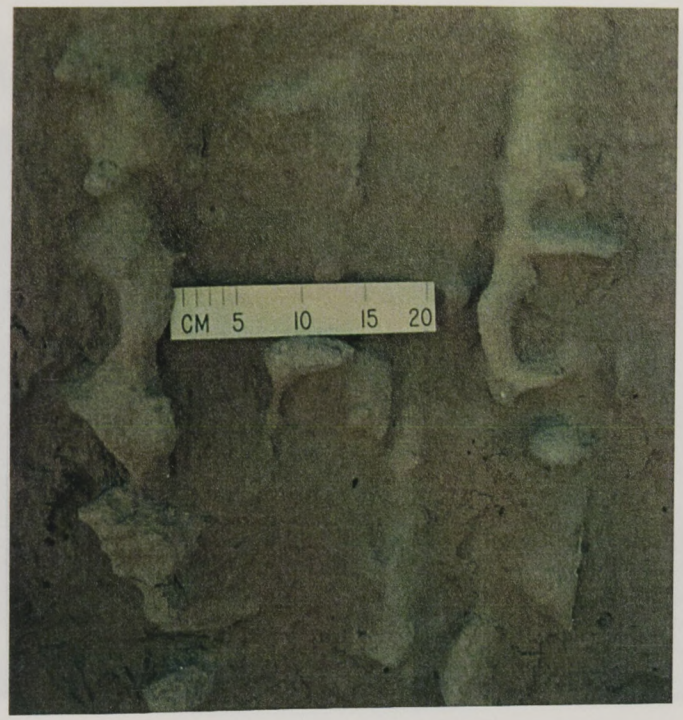

Figure 14. Elongate concretions perpendicular to bedding which are interpreted as rhizocretions. Bead Mountain, Arikaree Group.

Figure 15. Root in the field next to an elongate calcite-cemented concretion. Note similar morphology. Wildcat Hills, Arikaree Group.

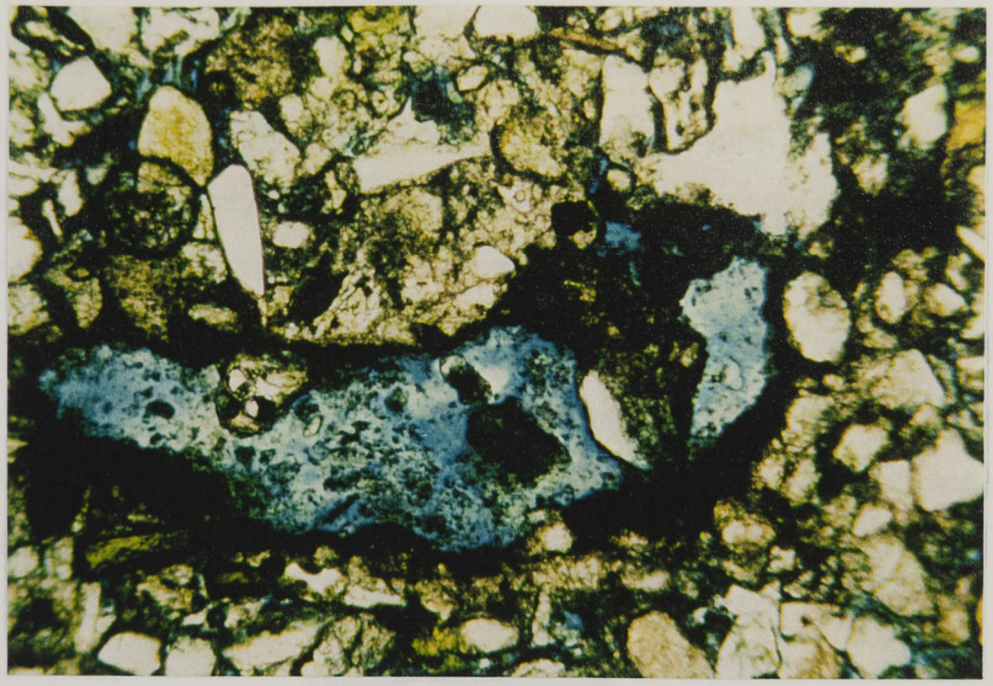

Figure 16. Photomicrograph of rhizocretion showing void lined with organic material. Field of view is 0.75 mm wide. North of Mitchel, Arikaree Group.

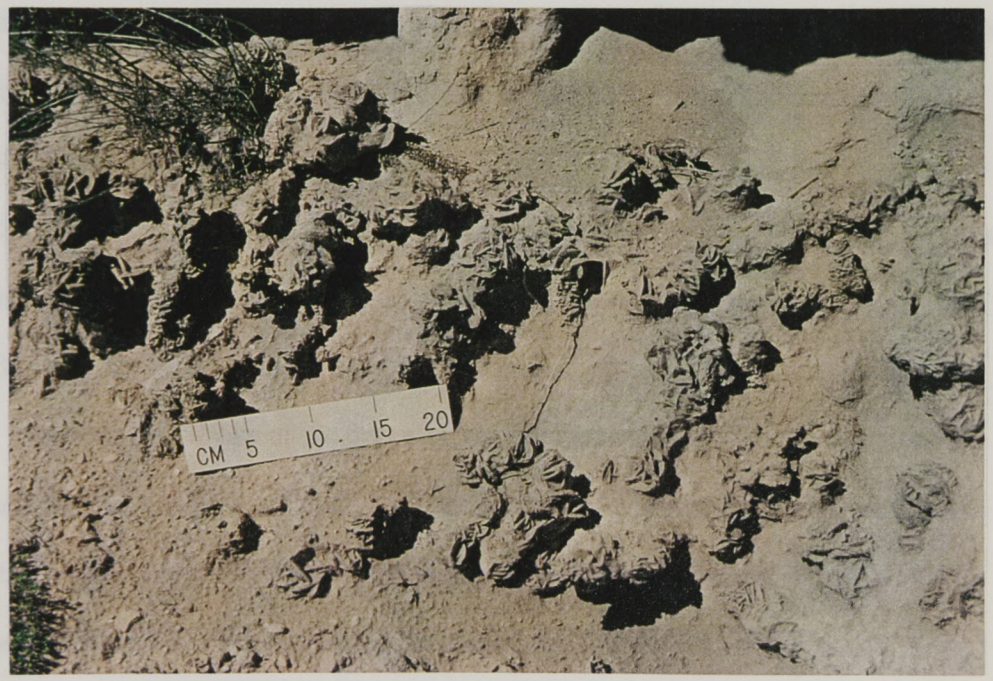

Figure 17. Gypsum rosettes pseudomorphed by calcite. Bead Mountain, Arikaree Group

These concretions are characterized by the presence of voids 1 - 5 mm in diameter which are commonly lined with organic material. Original bedding is disrupted and preferential grain alignment is discontinuous. The range of carbon isotope values is $\delta^{13}C$ -6.5‰ to $\delta^{13}C$ -7.8‰. The range of oxygen isotope values is $\delta^{18}O$ -9.1‰ to $\delta^{18}O$ -10.8‰. The average carbon and oxygen isotopic values are $\delta^{18}O$ -9.9‰ and $\delta^{13}C$ -7.2‰. If groundwater had a $\delta^{18}O$ value of - 10 SMOW, then calcite cement precipitated near 15 degrees Celsius (**Fig. 13**). The temperature of precipitation is consistent with a burial depth of less than 100 m (Gosnold, 1990).

Gypsum Pseudomorphs

Clusters of petal-shaped crystals that resemble gypsum desert roses (**Fig. 17**), but which are now composed of poikilotopic calcite, make up less than 1 percent of the concretions in the Arikaree. They were found at Bead Mountain and Scotts Bluff localities. Gypsum pseudomorphs occur as lenses 3 to 20 m wide and from 10 to 35 cm thick that define discrete stratigraphic horizons in eolian sands. Individual rosettes are rarely greater than 5 cm in diameter. Individual poikilotopes range in length from 0.5 to 5 cm and contain 60 to 65 percent sand grains.

The lensoidal shape of the deposits, the eolian character of the surrounding beds, and the morphology of the crystals are consistent with the origin of rosettes as evaporitic gypsum crystals that formed in interdune sabkas (Glennie, 1970 p. 19; Retallack, 1990 p. 47). The timing of the calcite replacement is unknown, but must have occurred soon after the precipitation of gypsum due to the unstable nature of gypsum.

A)

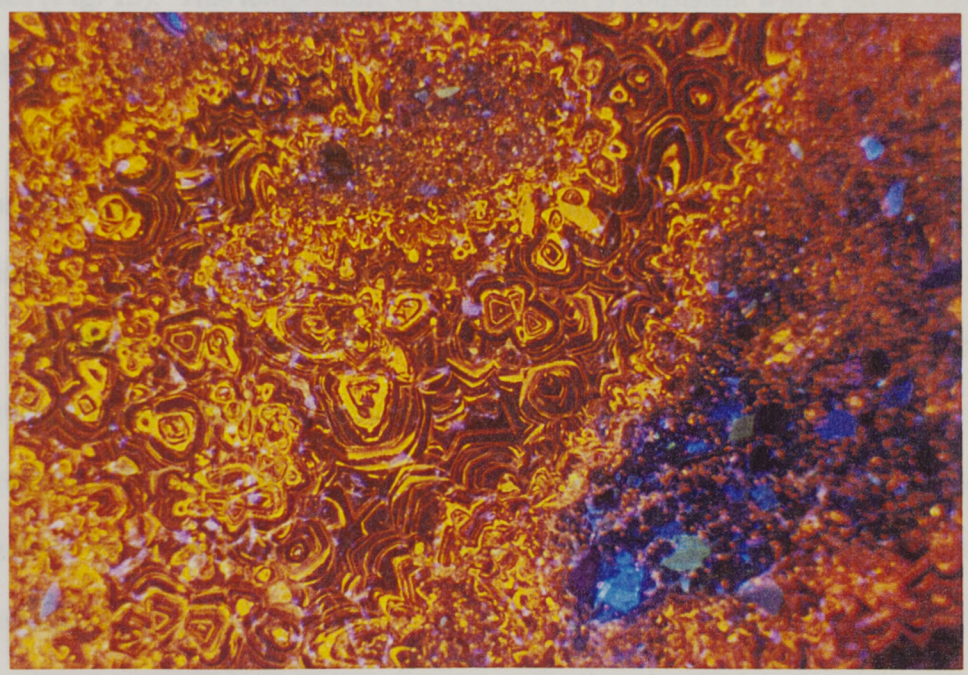

B)

Figure 18. **A)** Plain light and **B)** cathodoluminescence photomicrograph of gypsum pseudomorphs reflects variations in the chemistry or temperature of the cementing fluid. Blue epoxy fills pores. Field of view is 3.3 mm wide. Wildcat Hills, Arikaree Group.

The gypsum pseudomorphs have a dramatic cathodoluminescence pattern (**Fig. 18**) which shows complex cement stratigraphy. This pattern reflects precipitation or replacement during episodic changes in the chemistry or temperature of the cementing fluid.

No original bedding is visible in the rosettes and preferential grain alignment is discontinuous. These features are probably the result of disruption of original bedding by displacive gypsum precipitation. The range of carbon isotope values is $\delta^{13}C$ -6.5‰ to $\delta^{13}C$ -6.8‰. The range of oxygen isotope values is $\delta^{18}O$ -9.3‰ to $\delta^{18}O$ -9.7‰. The average carbon and oxygen isotopic values are $\delta^{18}O$ -9.5‰ and $\delta^{13}C$ -6.6‰. If groundwater had a $\delta^{18}O$ value of - 10 SMOW, then calcite cement precipitated near 15 degrees (**Fig. 13**). This temperature of precipitation is consistent with a burial depth of less than 100 m (Gosnold, 1990).

Forms Generated by Fluid Flow in the Phreatic Zone: Elongate Forms Parallel With Bedding

Elongate concretions parallel with bedding make up 65 to 80 percent of the total concretions in the Arikaree Group and have traditionally been called "pipy concretions." The term "pipy concretion" is misleading because the concretions are not hollow. However, the term has been used since Barbour (1900) first described the concretions.

Pipy concretions are highly elongate, well aligned, cylindrical masses which are generally tapered on both ends and range in diameter from 2 to 50 cm and from 3 cm to 35 m in length. Pipy concretions occur as isolated individual pipes, regular laterally

spaced pipes in particular stratigraphic horizons (**Fig. 19**), and as laterally linked bodies which form locally continuous sheets (**Fig. 20**). The vertical distance between pipe-rich layers varies greatly and ranges from 20 cm to 7 m. In several places the concretions are so closely spaced vertically that they merge to form laterally discontinuous masses 0.5 to 1 m thick (**Fig. 21**). Pipy concretions occur in eolian sands throughout the Arikaree Group and in high energy fluvial sands at Rattlesnake Butte. They are always elongate and often symmetrical about the elongate axis. They locally cut across foresets and inclined laminations in cross-stratified and ripple-cross-laminated beds (**Fig. 22**). The presence of aligned concretions in beds with different types of stratification (parallel lamination, cross-beds) suggests that sedimentary structures do not control concretion orientation.

The pipy concretions and the fabric of the adjacent uncemented host sand ranges from no alignment of framework grains to strong preferential alignment of elongate grains. The range of carbon isotope values is $\delta^{13}C$ -5.9‰ to $\delta^{13}C$ -8.1‰. The range of oxygen isotope values is $\delta^{18}O$ -10.0‰ to $\delta^{18}O$ -12.1‰. The average carbon and oxygen isotopic values are $\delta^{18}O$ -10.8‰ and $\delta^{13}C$ -7.1‰. If groundwater had a $\delta^{18}O$ value of - 10 SMOW, then calcite cement precipitated near 18 degrees (**Fig. 13**). This temperature of precipitation is consistent with a burial depth of less than 100 m (Gosnold, 1990).

The orientation of the pipy concretions is remarkably uniform at any one field locality. I made measurements of the axial trends of 9 to 45 pipy concretions per field locality and found a maximum standard deviation of less than 14 degrees (**Fig. 23**). Schultz (1941) took one axial trend measurement at many field localities and plotted

them on a regional map. When plotted together, Schultz's data and mine are consistent and show that concretions generally trend east-west, but change orientation in the vicinity of crystalline basement outcrops (**Fig. 24**). Changes in orientation around these outcrops were attributed by Schultz (1941) to the deflection of groundwater flow direction. Because the east-west orientation of most pipy concretions coincides with the regional slope of the Great Plains, Schultz (1941) concluded that the concretions

Figure 19. Individual pipy concretions occurring preferentially in discrete stratigraphic horizons at the Pine Ridge locality.

A)

B)

Figure 20. **A**) Laterally linked bodies which form complex anastomosing forms in the plane of bedding. View is looking down at concretions. Toe of boot shows scale. **B**) Laterally linked bodies locally forming continuous sheets. Hammer under ledge shows scale. Bead Mountain, Arikaree Group.

Figure 21. Closely spaced concretions merging vertically to form laterally discontinuous masses. Hammer shows scale. Wildcat Hills West, Arikaree Group.

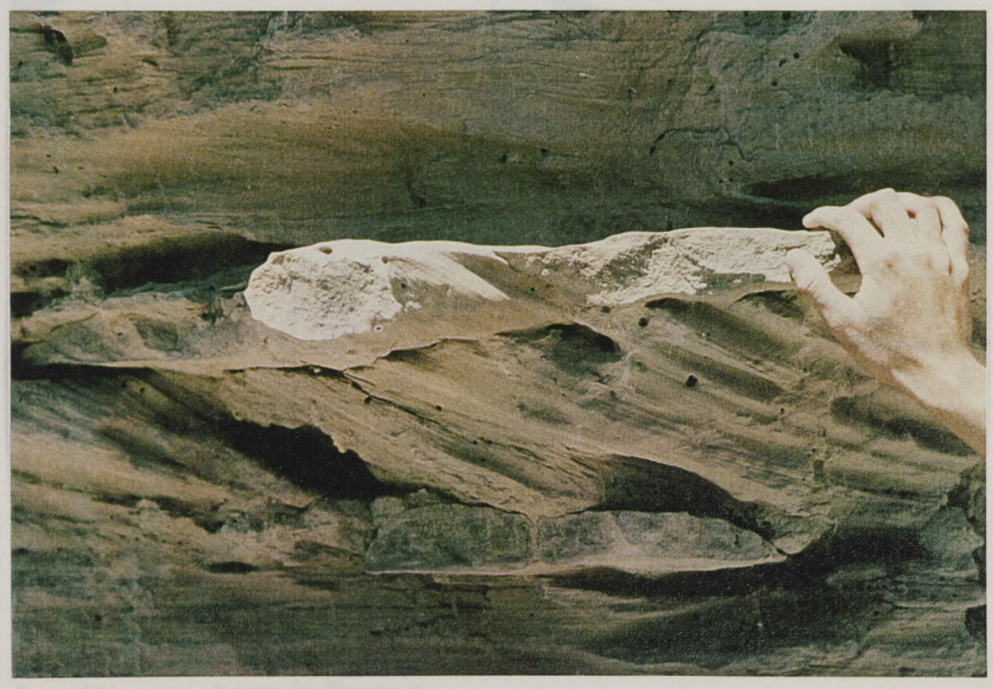

Figure 22. Horizontal elongate concretions in the plane of bedding cutting cross-stratified and ripple-cross-laminated beds. Scotts Bluff National Monument, Arikaree Group.

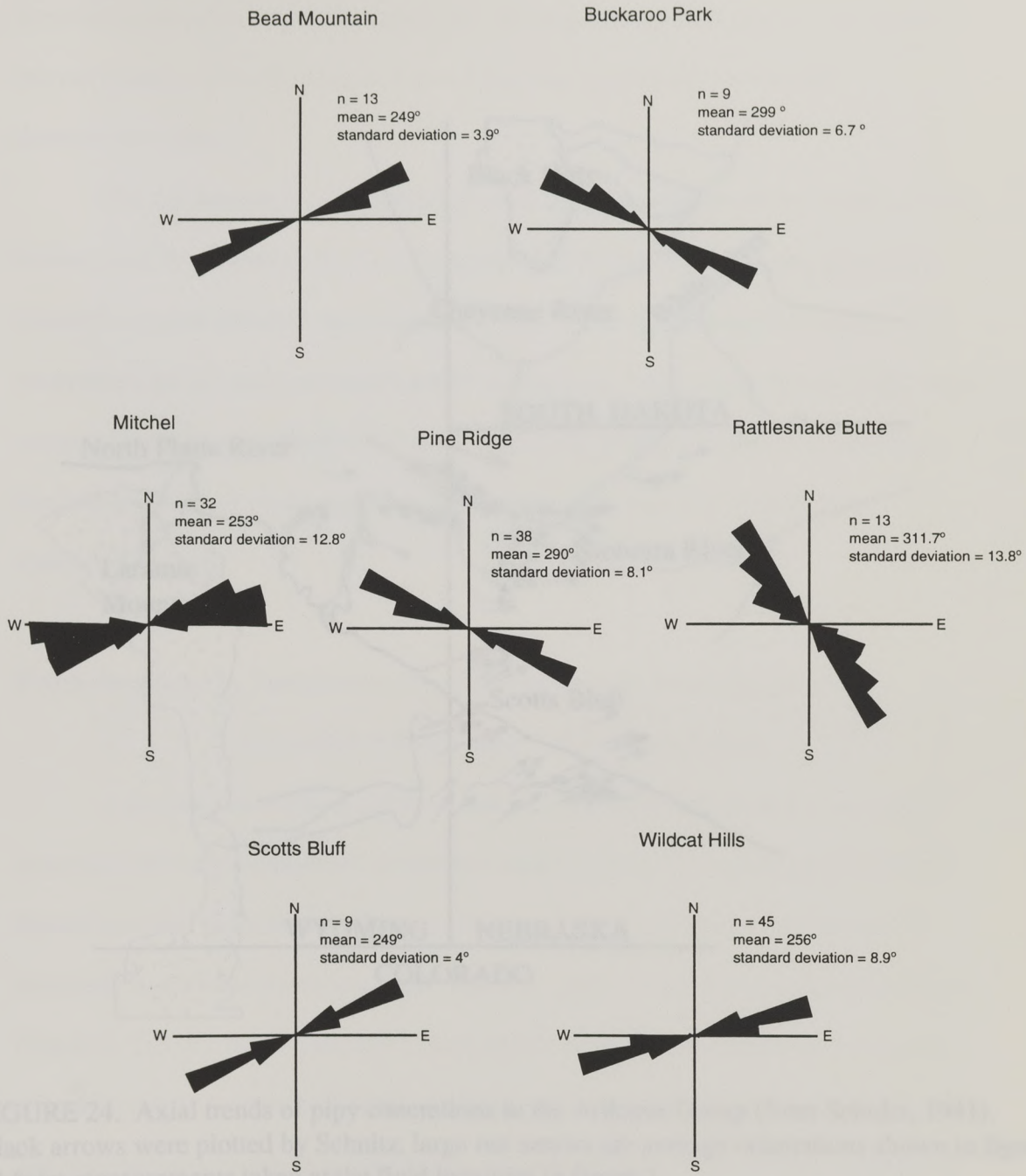

Figure 23. Rose diagrams of the axial trends of the long axis of pipy concretions. Localities are shown in figure 1.

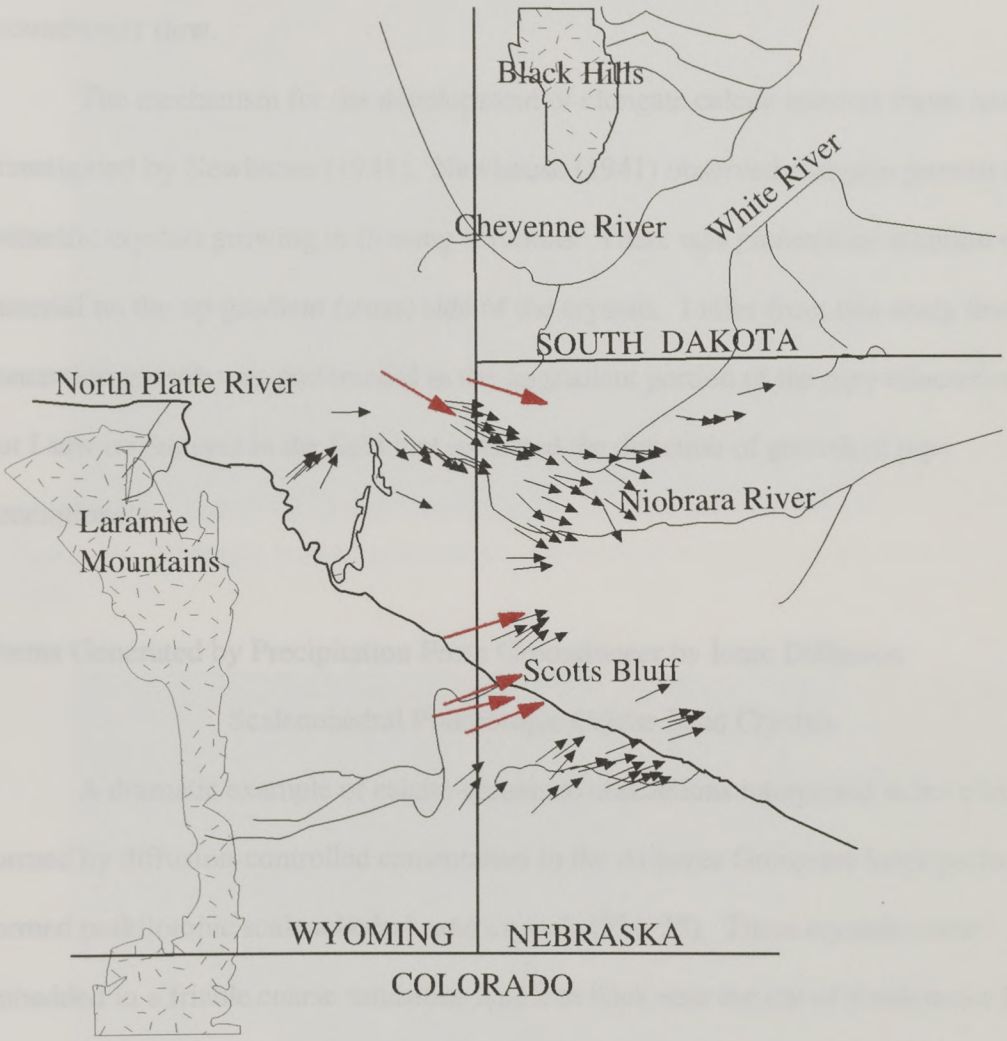

FIGURE 24. Axial trends of pipy concretions in the Arikaree Group (from Schultz, 1941). Black arrows were plotted by Schultz, large red arrows are average orientations shown in figure 23 from measurements taken at the field localities in figure 1.

grew in the direction of groundwater flow. Because the regional topographic gradient has not changed since the Miocene, presumably neither has the direction of groundwater flow.

The mechanism for the development of elongate calcite mineral forms has been investigated by Newhouse (1941). Newhouse (1941) observed elongate growth in isometric crystals growing in flowing solutions. There was preferential addition of material on the up-gradient (stoss) side of the crystals. I infer from this study that pipy concretion growth was preferential in the upgradient portion of the pipy concretions, but I saw no features in the field that indicated the direction of growth of pipy concretions.

Forms Generated by Precipitation From Groundwater by Ionic Diffusion

Scalenohedral Poikilotopic Calcite Sand Crystals

A dramatic example of calcite-cemented concretions interpreted to have been formed by diffusion-controlled cementation in the Arikaree Group are large perfectly formed poikilotopic scalenohedral sand crystals (**Fig. 25**). These crystals occur imbedded in a friable coarse sandstone lens 2 m thick near the top of Rattlesnake Butte (**Fig 26**). The crystals are six sided, blunt ended, doubly terminated, scalenohedrons (**Fig. 27**), which occur as individual crystals 1 to 20 cm in length, as clusters of 2 to 30 interpenetrating crystals (**Fig. 28**), and as more complex compound forms composed of 100 or more interpenetrting crystals. Some of the crystals have curved faces, while others have almost perfect scalenohedral forms with an average length from 1 to 15

Figure 25. Perfectly formed poikilotopic scalenohedral sand crystals from Rattlesnake Butte.

Figure 26. Rattlesnake Butte, Pine Ridge Indian Reservation, South Dakota. Arikaree Group.

cm. Each sand crystal is a single crystal of calcite (poikilotope), with an IGV of close to 37 percent.

These poikilotopes enclose variable-sized framework grains ranging from silt to clasts 3 cm in diameter. Sand crystals show no preferred orientation in outcrop. Some of the more weathered crystals are found in bedding planes of the sandstone host (**Fig. 29**), while others crop out as radiating sunburst patterns on broken surfaces (**Fig. 30**). Original sedimentary bedding is undisturbed and is either laminated or crossbedded.

There are several explanations for the formation of scalenohedral sand calcite crystals with curved crystal faces. Perfect scalenehedral sand crystals have been grown experimentally at high superstaturation (Kostov, 1968). The presence of curved faces and corners implies special conditions of growth beyond high supersaturation. Cailleau (1980) described the precipitation of crystals of calcite with ovoidal forms about 6μ long in solutions with a high ratio of Mg/Ca. Folk (1974) has also described a retarding effect of Mg^{++} on calcite growth. This retarding effect could create the appearance of curved faces. Bustillo, Escorza, and Clemente (1982) suggest that during the process of growth, normal scalenohedral faces encounter sand grains and are not able to push them away, causing the faces to break in sectors. These sectors grow through the free space between grains. The high supersaturation causes these sectors to grow quickly, depriving the crystals of the opportunity to reconstruct the scalenohedron morphology. Cody (1991) has shown experimentally that crystal habit may be modified by organic inhibitor molecules. A similar process may have occurred at

Figure 27. Idealized ditrigonal scalenohedron. Modified from Klein and Hurlbut, 1985.

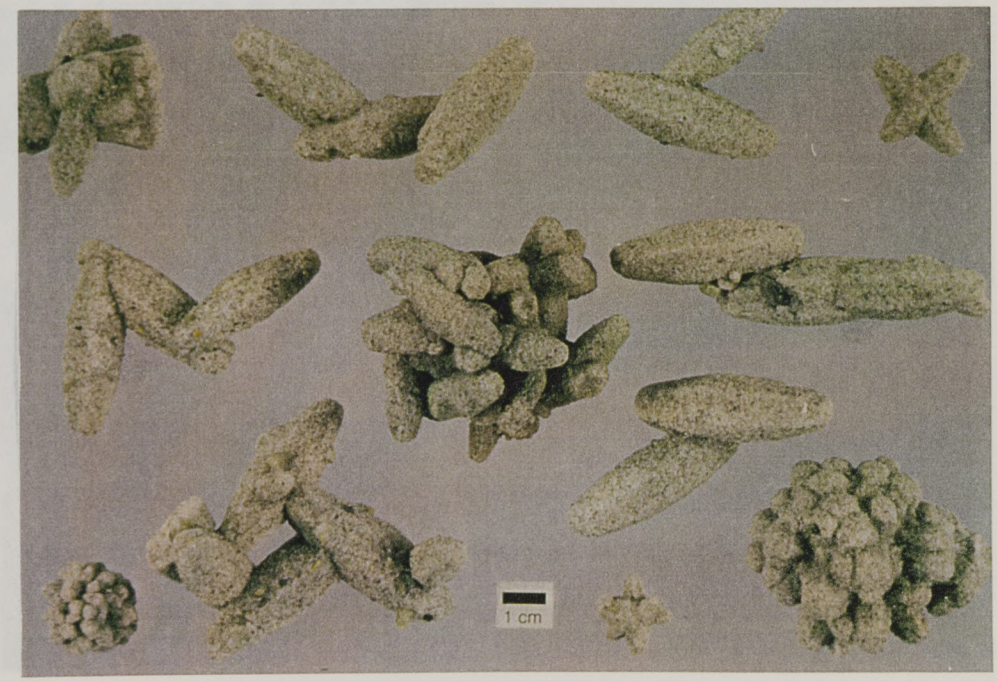

Figure 28. Complex interpenetrant compound scalenohedral forms at Rattlesnake Butte.

Figure 29. Some of the more weathered exposures at Rattlesnake Butte show bedding planes of the sandstone host with no preferred orientation of sand crystals.

Figure 30. Radiating sunburst pattern at Rattlesnake Butte.

Rattlesnake Butte in the presence of particular organic acids that were responsible for the formation of curved faces in scalenohedral poikilotopes.

The range of carbon isotope values for forms generated by diffusion at Rattlesnake Butte is $\delta^{13}C$ -8.6‰ to $\delta^{13}C$ -9.2‰. The range of oxygen isotope values is $\delta^{18}O$ -12.0‰ to $\delta^{18}O$ -13.4‰.

Spheres

Equant spherical concretions and oblate spheroids 5 to 30 cm in diameter occur at Rattlesnake Butte. Often they are interpenetrant and form clusters 2 to 3 m wide of 3 to 35 spheres (**Fig. 31**). 15 percent of the spheres contain carbonate rock fragments, some of which are pipy concretions. The clasts may have acted as nuclei for spherical concretion precipitation. Fabric and carbon and oxygen isotope values are similar to poikilotopic scalenohedral sand crystals suggesting that they formed under similar temperature and burial conditions.

Spherical Buckaroo Concretions

Spherical concretions 1 to 5 cm in diameter were found at the Buckaroo Park locality. These concretions formed clusters of 2 to 10 spheres which are not interpenetrant. The spheres are concentrically layered with alternating zones several mm thick of cemented and uncemented sands (**Fig. 32**). Manganese oxide grain coats (mangans) are common around all framework grains at Buckaroo Park and compose 0.5 percent of the material present. Original bedding is disrupted and preferential grain alignment is discontinuous. The range of carbon isotope values is $\delta^{13}C$ -8.0‰ to

Figure 31. Interpenetrant clusters of spheres at Rattlesnake Butte, Arikaree Group.

Figure 32. Spheres with concentric alternating zones of cemented and uncemented sands. Arikaree Group, Buckaroo Park, Wyoming.

$\delta^{13}C$ -8.1‰. The range of oxygen isotope values is $\delta^{18}O$ -12.0‰ to $\delta^{18}O$ -13.4‰. The average carbon and oxygen isotopic values are $\delta^{18}O$ -12.7‰ and $\delta^{13}C$ -8.1‰. If groundwater had a $\delta^{18}O$ value of - 10 SMOW, then calcite cement precipitated near 27 degrees (**Fig. 13**). This temperature of precipitation is consistent with a burial depth of 150-180 m (Gosnold, 1990).

CARBON AND OXYGEN ISOTOPES

Authigenic calcite was characterized by an analyses of stable carbon and oxygen isotopes of 40 concretion samples (**Fig. 33**) and adjacent host sands. The concretions analyzed contain no carbonate rock particles, so whole-rock analyses reflect the composition of authigenic calcite. Isotopic values for the host sandstone were attempted, but no calcite was present. In order to determine whether isotopic/temperature conditions were uniform during concretion growth or whether they changed with time, a pipy concretion was sampled in four regularly spaced intervals. The differences between adjacent samples differ by less than 0.5‰ in $\delta^{18}O$ and less than 0.6‰ in $\delta^{13}C$, indicating that geochemical conditions were stable during concretion growth.

The $\delta^{13}C$ values for concretions range from -9.2‰ to -5.9‰ (PDB) and form two clusters of data points (**Fig. 33**). Concretions interpreted to have formed by precipitation from groundwater by ionic diffusion have an average $\delta^{13}C$ of -8.7‰, while forms interpreted to have precipitated by surficial vadose processes and fluid flow through the phreatic zone have an average $\delta^{13}C$ of -7.0‰.

Based on the mineral assemblage, the lack of carbonate rock fragments, the lack of reduced iron or manganese, and the absence of marine skeletal material, I interpret these values to reflect the incorporation of organic CO_2 released by bacterial oxidation of organic material near the surface where oxygen was freely available. The cluster of more depleted data points represents samples whose carbon was also the result of bacterial oxidation, but may reflect greater incorporation of organically derived CO_2.

The $\delta^{18}O$ values for concretions range from -8.5‰ to -13.6‰ (SMOW) and form two clusters of data points (**Fig 33**). $\delta^{18}O$ of concretions interpreted to have formed by surficial processes and fluid flow in the phreatic zone have average $\delta^{18}O$ of -10.4‰, while forms interpreted to have formed by ionic diffusion have an average $\delta^{18}O$ of -12.7‰. Assuming that the $\delta^{18}O$ of rain in this region was -9‰ to -11‰ (SMOW) (Yurtsever, 1975), concretions interpreted to have formed by diffusion precipitated at 25 to 30 degrees Celsius, whereas concretions interpreted to have formed by fluid flow in the phreatic zone and by surficial vadose processes precipitated between 15 and 20 degrees Celsius (**Fig. 13**). The variation in temperature of precipitation suggests that forms interpreted to have precipitated by ionic diffusion precipitated in an environment consistent with 150 to 200 m of burial (Gosnold, 1990), whereas forms interpreted to have formed by fluid flow in the phreatic zone and by surficial processes precipitated in an environment consistent with less than 100 m of burial (Gosnold, 1990).

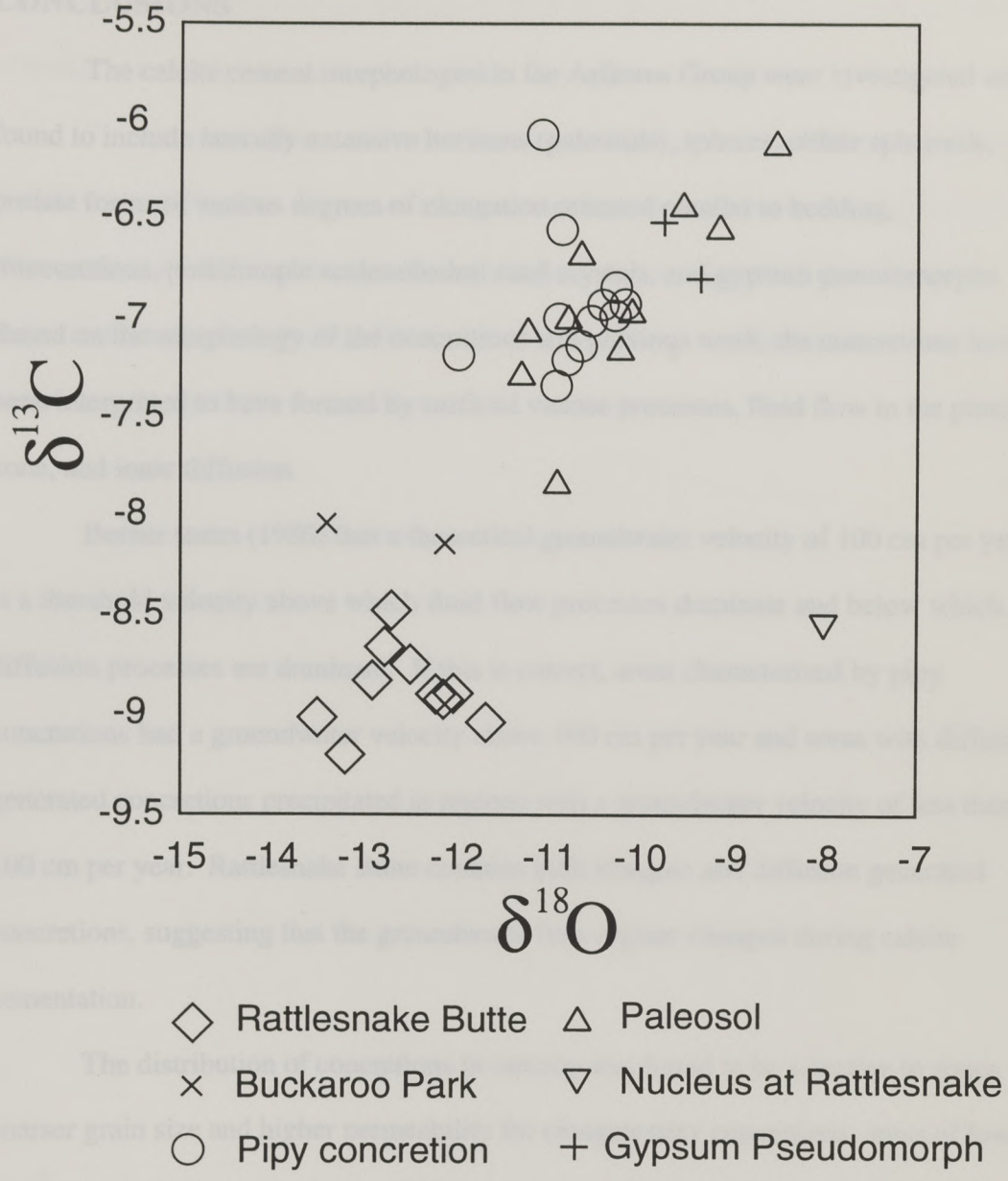

Figure 33. Carbon and oxygen isotope analyses of calcite cemented concretions of the Arikaree Group.

CONCLUSIONS

The calcite cement morphologies in the Arikaree Group were investigated and found to include laterally extensive horizons (paleosols), spheres, oblate spheroids, prolate forms of various degrees of elongation oriented parallel to bedding, rhizocretions, poikilotopic scalenohedral sand crystals, and gypsum pseudomorphs. Based on the morphology of the concretions and previous work, the concretions have been interpreted to have formed by surficial vadose processes, fluid flow in the phreatic zone, and ionic diffusion.

Berner states (1980) that a theoretical groundwater velocity of 100 cm per year is a threshold velocity above which fluid flow processes dominate and below which diffusion processes are dominant. If this is correct, areas characterized by pipy concretions had a groundwater velocity above 100 cm per year and areas with diffusion generated concretions precipitated in regions with a groundwater velocity of less than 100 cm per year. Rattlesnake Butte contains both elongate and diffusion generated concretions, suggesting that the groundwater flow regime changed during calcite cementation.

The distribution of concretions in outcrop was found to be selective to zones of coarser grain size and higher permeability for elongate pipy concretions, areas of lower interstitial fluid flow velocity for diffusion generated forms, and areas which were pedogenic horizons for forms generated by normal surficial vadose processes.

Oxygen isotopes indicate that forms interpreted to have formed by diffusion precipitated at a temperature which is consistent with 150 - 200 m of burial. Forms interpreted to have formed by surficial vadose processes and fluid flow in the phreatic

zone are inferred from oxygen isotopes to have precipitated at depths less than 100 m of burial at temperatures consistent average atmospheric conditions.

Paleosols and rhizocretions are thought to have taken 10^3 to 10^4 years to form (Retallack, 1990 p.263). Pipy concretions are interpreted to have formed during the deposition of the Arikaree because clasts of pipy concretions are found in fluvial deposits at Rattlesnake Butte. The timing of replacement of gypsum deposits and diffusion generated forms is unknown.

Appendix A
Point count data

Sample	Concretion Type	Porosity	VRF	Shard	Heavy	Unknown	Unstained Calcite	Calcite Cement	Plag	Qtz	Opaque	Kspar	Twinned Plag
29E	pipy	9.7	21.7	6.0	3.0	1.0	7.3	28.0	4.3	10.7	5.7	0.0	2.7
29W	pipy	1.7	22.3	10.3	2.7	0.0	9.7	34.0	4.0	8.3	4.7	0.3	2.0
40	pipy	0.0	21.3	9.3	3.3	1.7	6.0	37.3	5.7	5.7	5.0	0.0	4.7
100	gyp pseudo	13.0	19.3	8.7	3.0	0.0	6.7	25.7	5.0	10.7	1.3	0.7	6.0
32	paleosol	0.0	21.7	9.7	2.7	0.3	2.7	42.7	8.3	10.0	0.3	0.0	1.7
4	pipy	0.0	33.3	4.8	2.1	0.7	6.2	30.6	5.8	12.4	3.8	0.3	0.0
41	pipy	1.3	26.0	7.0	4.0	0.0	9.3	31.7	5.3	10.3	4.7	3.0	0.0
57	pipy	28.0	29.3	9.3	2.0	1.0	0.0	0.0	18.0	11.0	1.3	0.0	0.0
58	host	31.0	19.7	9.3	3.7	1.0	0.0	0.0	17.7	13.3	4.0	0.3	0.0
6	pipy	0.0	19.9	8.7	2.4	0.0	9.1	43.7	11.5	4.2	0.3	0.0	0.0
48	host	40.0	33.3	4.7	4.0	1.0	0.0	0.0	10.0	6.3	0.7	0.0	0.0
54	host	34.3	25.3	6.7	4.7	1.3	0.0	0.0	14.7	10.7	2.3	0.0	0.0
12	lam. host	38.3	27.7	10.7	2.7	1.0	0.0	0.0	10.7	7.0	2.0	0.0	0.0
60	host	29.3	25.3	8.7	5.0	1.3	0.0	0.0	13.7	10.3	6.3	0.0	0.0
44	pipy	4.0	5.7	8.0	2.0	0.3	0.0	70.7	3.3	4.7	1.3	0.0	0.0
24	cement blob	1.3	7.3	8.0	4.3	0.3	0.0	59.0	7.3	10.3	2.0	0.0	0.0
35	host 24	35.3	19.0	7.7	5.7	1.0	0.0	0.0	14.3	14.3	2.7	0.0	0.0
47	rhizocretion	36.7	29.7	8.3	4.0	1.0	0.0	0.0	11.3	6.7	2.3	0.0	0.0
26	rhizocretion	39.3	21.0	9.7	4.0	0.3	0.0	0.0	12.7	10.7	2.3	0.0	0.0
27	host	38.3	19.7	9.0	5.3	0.0	0.0	0.0	13.7	13.0	1.0	0.0	0.0

Sample	Concretion Type	Porosity	VRF	Shard	Heavy	Unknown	Unstained Calcite	Calcite Cement	Plag	Qtz	Opaque	Kspar	Twinned Plag
46	paleosol	0.0	18.7	6.0	3.0	0.0	6.4	50.2	8.7	5.4	1.7	0.0	0.0
36	host	38.0	33.0	6.3	3.7	0.0	0.0	0.0	10.0	8.3	0.7	0.0	0.0
30	pipy	0.0	14.0	5.3	2.0	0.3	1.0	57.3	7.3	11.3	1.0	0.3	0.0
49	rhizocretion	39.3	26.2	7.8	1.2	0.0	0.0	0.0	7.5	6.9	2.8	0.9	7.5
42	pipy	0.0	17.1	9.4	2.7	0.3	1.3	47.2	7.7	12.7	1.7	0.0	0.0
59	host	42.3	25.3	7.7	3.0	0.0	0.0	0.0	8.0	11.7	1.7	0.3	0.0
27	resist host	41.7	23.2	8.9	2.0	0.3	0.0	0.0	6.3	16.2	1.0	0.3	0.0
21	rhizocretion	0.0	32.7	8.7	0.7	0.0	5.0	45.3	5.7	1.0	1.0	0.0	0.0
2	pipy	0.0	8.7	2.7	2.0	0.0	17.3	47.0	18.3	4.0	0.0	0.0	0.0
8	pipy	0.0	12.3	9.0	2.0	0.0	14.3	40.0	14.0	5.3	3.0	0.0	0.0

Appendix B
Carbon and oxygen isotope analysis

Sample	Concretion type	δ18-O	δ13-C
AIR-14	cemented horizon	-11.2	-7.1
AIR-16	cemented horizon	-10.1	-7.0
AIR-46	cemented horizon	-8.5	-6.1
WC-5	cemented horizon	-10.1	-7.0
avg		**-10.0**	**-6.8**
AIR-8	pipy	-12.1	-7.3
AIR-19	pipy	-10.1	-6.9
AIR-4	pipy	-10.7	-6.5
AIR-30	pipy	-10.2	-7.0
AIR-42	pipy	-10.6	-7.3
AIR-65	pipy	-11.0	-5.9
AIR-1A	pipy	-10.5	-7.3
AIR-1B	pipy	-10.4	-7.1
AIR-1C	pipy	-10.0	-7.0
AIR-1D	pipy	-10.8	-7.5
P-2	pipy	-10.7	-7.1
P-10C	pipy	-11.2	-7.6
P-10S	pipy	-11.8	-8.1
avg		**-10.8**	**-7.1**
AIR-101	gyp pseudo	-9.7	-6.5
AIR-68	gyp pseudo	-9.3	-6.8
avg		**-9.5**	**-6.6**
AIR-18	root	-10.8	-7.8
AIR-7	root	-9.1	-6.5
avg		**-9.9**	**-7.2**
AIR-24	blob	-10.6	-6.7
M-1	center blob	-8.9	-6.5
AIR-41	spheroidal	-10.5	-7.0
M-2	thin bed next to blob	-10.8	-7.0
avg		**-10.2**	**-6.8**
AIR-73	ash w calcite	-10.2	-7.1
RS-9	elongate	-12.8	-8.4

Sample	Concretion type	δ18-O	δ13-C
RS'-3	sphere	-12.6	-8.7
RS-3	sphere	-12.9	-8.8
RS'-2	sphere	-13.1	-9.2
R-0	sphere	-12.0	-8.9
POT-1	sxl	-12.4	-8.7
POT-2	sxl	-12.2	-8.9
R-2	sxl	-12.4	-8.7
RS-SXL	sxl	-12.2	-8.9
RS'-4	elongate	-12.6	-8.6
RS'-5	loaf	-13.4	-9.0
avg		**-12.6**	**-8.8**
RS'-4C	clast of pipy	-8.0	-8.5
B-3	Buckaroo sphere	-12.0	-8.1
B-1	Buckaroo sphere	-13.4	-8.0
	avg	**-12.7**	**-8.1**

Appendix C
Electron microprobe analysis of calcite cement
33 additional data points were analyzed, but were below detection limits for all trace elements.
BDL = Below detection limits

Sample	Concretion type	Data point	mol % Ca	mol % Mg	mol % Mn	mol % Sr	mol % Fe	mol % SiO2
AIR 46	paleosol	#1/3	99.00	BDL	0.69	BDL	BDL	BDL
		#2/1	99.25	0.68	BDL	BDL	BDL	BDL
		#2/3	98.70	0.52	BDL	BDL	BDL	0.53
		#2/6	99.43	0.54	BDL	BDL	BDL	BDL
		#3/1	99.48	0.44	BDL	BDL	BDL	BDL
		#3/5	99.59	0.37	BDL	BDL	BDL	BDL
		#3/6	98.89	0.53	BDL	BDL	BDL	0.66
AIR 42	pipy concretion	#1/1	98.86	BDL	0.79	BDL	BDL	BDL
		#1/2	99.29	0.45	BDL	BDL	BDL	BDL
		#1/3	99.46	0.39	BDL	BDL	BDL	BDL
		#2/2	99.21	0.53	BDL	BDL	BDL	BDL
		#2/4	99.34	0.53	BDL	BDL	BDL	BDL
		#3/1	99.54	0.33	BDL	BDL	BDL	BDL
		#3/2	99.50	0.4	BDL	BDL	BDL	BDL
AIR 21	rhizocretion	#1/1	99.51	0.38	BDL	BDL	BDL	BDL
		#2/1	99.44	0.35	BDL	BDL	BDL	BDL

Appendix D
ICP analysis of calcite cement

Sample	Concretion Type	mol % Ca	mol % Mg	mol % Mn	mol % Sr	mol % Fe
B-3	Sphere	99.45	0.49	0.03	0.00	0.02
GYP	Gypsum Pseudomorph	99.30	0.61	0.03	0.01	0.05
M-4	Paleosol	99.43	0.52	0.01	0.00	0.04
P-2	Pipy	98.68	0.94	0.32	0.01	0.05
RS-4	Sphere	99.23	0.70	0.05	0.00	0.02
RS-SXL	Scalenohedral Sand Xl	99.31	0.67	0.00	0.00	0.02
WC-5	Paleosol	98.97	0.91	0.07	0.01	0.04
42	Pipy	99.18	0.74	0.03	0.01	0.04

REFERENCES

Armstrong, R.L., 1968, Sevier orogenic belt in Nevada and Utah: Geological Society of America Bulletin, v. 79, p. 429-458.

Barbour, Erwin H., 1901, Sand crystals and their relation to certain concretionary forms: Geologic Society of America Bulletin, v. 12, p. 165-172.

Barbour, E.H., and Fisher, C.A., 1902, A new form of calcite sand crystal: American Journal of Science, v. 14, p. 451-454.

Bart, H.A., 1974, A sedimentological and petrographic study of the Miocene Arikaree Group of south-eastern Wyoming and west-central Nebraska, unpublished PhD. Thesis, Univ. Wyom, 106 p.

Bathurst, R.G.C., 1975, Carbonate sediments and their diagenesis: 2nd Ed., New York: Elsevier, 658 pp.

Berner, R. A., 1968, Rate of concretion growth: Geochim. Cosmochim. Acta, v. 32, p. 477-483.

Berner, R. A., 1980, Early diagenesis: a theoretical approach: Princeton, New Jersey, Princeton University Press 241p.

Blatt, Harvey, 1992, Sedimentary Petrology, W.H. Freeman, New York, 514 p.

Boles, J.R., and S.G. Franks, 1979, Clay diagenesis in smectite diagenesis on sandstone cementation: Journal of Sedimentary Petrology, v. 49, p. 55-70.

Boles, J.R., and Johnson, S., 1983, Influence of mica surface on pore-water pH: Chem. Geology, v. 43, p. 303-317.

Bjørkum, P.A., and Olav Walderhaug, 1990, Geometrical arrangement of calcite cementation within shallow marine sandstones: Earth-Sciences Reviews, v. 29, p. 145-161.

Bjørkum, P.A., and Olav Walderhaug, 1993, Isotopic composition of a calcite-cemented layer in the Lower Jurassic Birdport Sands, southern England: Implications for formation of laterally extensive calcite-cemented layers: Journal of Sedimentary Petrology, v. 63, p. 678-682.

Brewer, R., 1976, Fabric and mineral analysis of soils: New York, Krieger Publishers.

Bryant, I.D., Kantorowicz, J.D., and Love, C.F., 1988, The origin and recognition of laterally extensive continuous carbonate-cemented horizons in the Upper Lias Sands of southern England: Marine and Petroleum Geology, v. 5, p. 108-133.

Bustillo, M.A., Escorza, C.M., Clemente, R.R., 1982, Ovoidal calcite sand crystals from Miocene fluvial sediments: Estudios Geol., v. 38, p. 373-377.

Cailleau, P., Dragone, D., Esclamadon, J., Girou, A., Humbert, L., Roques, H., and Sellier, E., 1980, Cristallisation en milieu libre et en mileu poreux, dissolution et pression-dissolution: principaux resultats experimentaux: Reunion of Cristallisation-Deformation Dissolution des Carbonates, Bordeaux, p. 81-89.

Campbell, F.H., and Mitchell, R.S., 1961, Sand-calcite crystals from Stoneham, Colorado: Rocks and Minerals, v. 36, p. 18-21.

Cerling, T.E., 1984, The isotopic composition of modern soil carbonate and its relation to climate: Earth Planetary Sci. Letters, v. 71, p. 229-240.

Cerling, T.E. and Hay, R., 1986, An isotopic study of paleosol carbonates from Olduvai Gorge: Quaternary Research, v. 25, p. 63-78.

Clark, J., Beerbower, J.R., and Kietzke, K.K., 1967, Oligocene sedimentation, stratigraphy, paleoecology and paleoclimatology in the Big Badlands of South Dakota: Fieldiana-Geology, v. 5, p. 5-158.

Cody, R.D., 1991, Organo-crystalline interactions in evaporite systems: the effects of crystallization inhibition: Journal of Sedimentary Petrology, v. 61, No. 5, p. 704-718.

Coleman, M.L., 1993, Microbial processes: controls on the shape and composition of carbonate concretions: Marine Geology, v. 113, p. 127-140.

Coleman, M.L. and Raiswell, R., 1981, Carbon, oxygen and sulfur isotope variations in concretions from the Upper Lias of N.E. England: Geochima et Cosmochimica Acta, v. 45, p. 329-340.

Colton, G.W., 1967, Orientation of carbonate concretions in the Upper Devonian of New York: U.S. Geological Survey Professional Paper 575-B, p. B57-B59.

Coniglio, M., and Cameron, J.S., 1990, Early diagenesis in a potential oil Shale: evidence from calcite concretions in the Upper Devonian Kettle Point Formation, southwestern Ontario: Bulletin of Canadian Petroleum Geology, v. 3, p. 64-77.

Connolly, J.P., 1930, The sand-calcite crystals of Devils Hill: The Black Hills Engineer, v. 18, p. 264-273.

Curtis, C.D., 1977, Sedimentary geochemistry: environments and processes dominated by involvement of an aqueous phase: Philosophical Transactions, Royal Soc. London, v. 286A, p. 353-372.

Curtis, C.D., and Coleman, M.L., 1986, Controls on the precipitation of early diagenetic calcite, dolomite and siderite concretions in complex depositional sequences, in D.L. Gautier (ed.): Roles of organic matter in sediment diagenesis, Soc. Econ. Paleontologists and Mineralogists, Spec. Pub No. 38, p. 23-34.

Davies, D.K., 1969, Shelf sedimentation: an example from the Jurassic of Britain: Journal of Sedimentary Petrology, v. 39, p. 1344-1370.

Deegan, C.E., 1971, The mode of origin of some late diagenetic sandstone concretions from the Scottish Carboniferous. Scott. Journal of geology, v. 7, p. 357-365.

Denson, N.M., and Bergendahl, N.H., 1961, Middle and Upper Tertiary rocks of southeastern Wyoming and adjoining areas: U.S. Geologic Survey Prof. Paper 424-C, p. 168-172.

Denson, N.M., and Botinelly, T., 1949, Geology of the Hartville Uplift, eastern Wyoming: U.S. Geol. Survey Oil and Gas Inv. Prelim. Map 102.

Denson, N.M., 1969, Distribution of nonopaque heavy minerals in Miocene and Pliocene rocks of central Wyoming and parts of adjacent states: U.S.G.S. Prof. Paper 650-C, p. C25-C32.

Denson, N.M. and W.A. Chisholm, 1971, Summary of mineralogic and lithologic characteristics of Tertiary sedimentary rocks in the middle Rocky Mountains and the northern Great Plains: U.S.G.S. Prof. Paper 750-C, p. C117-C126.

Drever, J., 1988, The geochemistry of natural waters, Englewood Cliffs, NJ, Prentice-Hall, Edition 2, 437 p.

Fastovsky, D.E., and Dott, R.H., 1986, Sedimentology, stratigraphy, and extinctions during the Cretaceous-Paleogene transition at Bug Creek, Montana: Geology, v. 14, p. 279-282.

Folk, R.L., 1968, Petrology of Sedimentary Rocks: Austin, Texas, Hemphill's, 170 p.

Folk, R.L., 1974, The natural history of crystalline calcium carbonate: effect of Mg content and salinity: Journal of Sedimentary Petrology, v. 44, p. 40-53.

Folk, R.L., Picard, M.D., and McBride, E.F., 1993, Highly elongate concretions in sandstone: evidence of paleoflow directions in groundwater (abstract): International Association Sedimentologists 14th Regional Meeting, Marrakesh, p. 8.

Fraser, H.J., 1935, Experimental study of the porosity and permeability of clastic sediments: Journal of Geol., v. 43 (8), p. 910-1010.

Fürsich, F.T., 1982, Rhythmic bedding and shell bed formation in the Upper Jurassic of East Greenland: *in* Einsele, G., and S. Seilacher (Eds), Cyclic and Event Stratification, Springer, Berlin, p. 208-222.

Glennie, K.W., 1970, Desert Sedimentary Environments: Amsterdam, The Netherlands, Elsevier Publishing, 222 pp.

Gluyas, J.G., 1984, Early carbonate diagenesis within Phanerozoic shales and sandstones of NW European shelf: Clay Minerals, v. 19, p. 309-321.

Gosnold, W.D., 1990, Heat flow in the Great Plains of the United States: Journal of Geophysical Research, v.95, No. B1, p. 353-374.

Hoveland, M., Talbot, M.R., Qvale, H., Olaussen, S., and Aasberg, L., 1987, Methane-related carbonate cements in pockmarks of the North Sea: Journal of Sedimentary Petrology, v. 57, p. 881-892.

Hudson, J.D., 1975, Carbon isotopes and limestone cement: Geology, v. 3, p. 19-22.

Hudson, J.D., and Andrews, J.E., 1987, The diagenesis of the Great Estuarine Group, Middle Jurassic, Inner Hebrides, Scotland: *in* Marshall, J.D., Diagenesis of Sedimentary Sequences: Geol. Society Special Pubs. No. 36, p. 259-276.

Hunt, R.H. Jr., 1981, Geology and vertebrate paleontology of the Agate Fossil Beds National Monument and surrounding region, Sioux County, Nebraska (1972-1978): National Geographic Society Research Reports, v. 13, p. 263-285.

Jacob, A.F., 1973, Elongate concretions as paleochannel indicators, Tongue River Formation (Paleocene), North Dakota: Geological Society of America Bulletin, v. 84, p. 2127-2132.

James, W.C., 1985, Early diagenesis, Atherton Formation (Quaternary): a guide for understanding early cement distribution and grain modifications in non-marine deposits; Journal of Sedimentary Petrology, v. 55, p. 135-146.

Johnson, M.R., 1989, Paleogeographic significance of oriented calcareous concretions in the Triassic Katberg Formation, South Africa: Journal of Sedimentary Petrology, v. 59, p. 1008-1010.

Kantorowicz, J.D., I.D. Bryant, and J.M. Dawans, 1987, Controls on the permeability and distribution of carbonate cements in Jurassic sandstones; Birdport Sands, southern England and Viking Group, Troll Field, Norway: *in* Marshal, J.D. (Ed.), Diagenesis of Sedimentary Sequences; Geol. Society Special Publications No. 36, p. 103-118.

Klien, C., and Hurlbut, C., 1985, Manual of mineralogy, 20th edition: John Wiley and Sons, New York, 596 p.

Kostov, I., 1968, Mineralogy: Oliver and Boyd, English Edition, 587 p.

Lacroix, A., 1901, Mineralogie de la France: Paris, France, v. 3, p. 515-517.

Lundegard, P.D., 1989, Temporal reconstruction of sandstone diagenetic histories: *in* Hutcheon, I.E. (Ed.), Burial Diagenesis: Minerealogical Association of Canada Short Course Handbook 15, p. 161-200.

Lundegard, P.D., and Land, L.S., 1986, Carbon dioxide and organic acids: their role in porosity enhancement and cementation, in D.L. Gautier (ed.): Roles of organic matter in sediment diagenesis, Soc. Econ. Paleontologists and Mineralogists Spec. Pub. No. 38, p. 129-146.

McBride, E.F., 1978, Reservoir aspects of submarine fan facies: example of the Marnosoarenacea Formation, Northern Apennines, Italy: Offshore Technology Conference Preprints; Houston, Texas, p. 587-591.

McBride, E.F., 1978, Porosity loss in sandstone by ductile grain deformation during compaction: Trans., Gulf Coast Assoc. Geol. Societies, v. 28, p. 323-325.

McBride, E.F., 1988, Contrasting diagenetic histories of concretions and host rock, Lion Mountain Sandstone (Cambrian), Texas: Geol. Soc. America Bull., v. 100, p. 1803-1810.

McBride, E.F., 1989, Quartz cement in sandstones: a review: Earth-Science Reviews, v. 26, p. 69-112.

McBride, E.F., Picard, M.D., and Folk, R.L., 1994, Oriented concretions, Ionian Coast, Italy: Evidence of groundwater flow direction: Journal of Sedimentary Research, v. A64, p. 535-540.

McKenna, M.C., 1965, Stratigraphic nomenclature of the Miocene Hemingford Group, Nebraska: American Museum Novitates, No. 2228, 21 p.

Meschter, D.Y., 1958, A study of concretions as applied to the geology of uranium deposits: U.S. Atomic Energy Commission Technical Memorandum Report TM-D-1-14, 10 p. (Available on microfiche from the U.S. Geological Survey in Denver.)

Mozley, P.S., and S.J. Burns, 1993, Oxygen and carbon isotopic composition of marine carbonate concretions: an overview: Journal of Sedimentary Petrology, v. 63, p. 73-83.

Mozley, P.S., and Davis, M.J., Relationship between oriented calcite concretions and permeability correlation structure in an alluvial aquifer, Sierra Ladrones Formation, New Mexico: Journal of Sedimentary Research, in press.

Osterwald, F.W., and Dean, B.G., 1957, Preliminary tectonic map of northern Colorado and northeastern Utah showing distribution of uranium deposits: U.S. Geol. Survey Mineral Inv. Map MF-130.

O'Harra, C.C., 1920, The White River Badlands: Bul. So. Dak. School of Mines, No. 13, 181 pp.

Parsons, M.W., 1980, Distribution and origin of elongate sandstone concretions, Bullion Creek and Slope Formations (Paleocene), Adams County, North Dakota [unpubl. MS thesis]: University of North Dakota, Grand Forks, North Dakota, 133 p.

Pettijohn, F.J., P.E. Potter, and Raymond Siever, 1987, Sand and Sandstone: Springer-Verlag, New York, 553 p.

Pettyjohn, W.A., 1966, Eocene paleosol in the northern Great Plains: U.S. Geol. Survey Prof. Paper 550-C, 61-65.

Pirrie, D., 1987, Oriented calcareous concretions from James Ross Island, Antarctica: British Antarctic Survey Bull., No. 75, p. 41-50.

Raiswell, R, 1971, The growth of Cambrian and Liassic concretions: Sedimentology, v. 17, No. 3-4, p. 147-171.

Raiswell, R. and White, N.J.M., 1978, Spatial aspects of concretionary growth in the upper Lias of Northeast England: Sed. Geology, v. 20, p. 291-300.

Retallack, G.J., 1990, Soils of the Past: University of Oregon, Eugene, 520 pp.

Retallack, G.J., 1983, Late Eocene and Oligocene paleosols from Badlands national Park, South Dakota: geological Society of America, Special Paper 193, 82 p.

Saigal, G. C. and K. Bjorlykke, 1987, Carbonate cements in clastic reservoir rocks from offshore Norway-relationships between isotope composition, textural development and burial depth: in Marshall, J.D. (ed.), Diagenesis of Sedimentary Sequences, Geol. Soc. Special Publ. No. 36, p. 313-324.

Sato, Y., and Denson, N.H., 1967, Volcanism and tectonism as reflected by the distribution of nonopaque heavy minerals in some Tertiary rocks of Wyoming and adjacent states: U.S. Geological Survey Professional Paper 575-C, p. 42-54.

Schultz, C.B., 1941, The pipy concretions of the Arikaree: Bull. Univ. Nebraska State Museum, v. 2, p. 69-82.

Sharp, J.M., and E.F. McBride, 1989, Sedimentary petrology- a guide to paleohydrogeologic analyses, examples of sandstones from northwest Gulf of Mexico: Journal of Hydrology, v. 108, p. 367-386.

Skinner, M.f., Skinner, S.M., and Gooris, R.J., 1977, Stratigraphy and biostratigraphy of Late Cenozoic deposits in central Sioux County, Nebraska: American Museum of Natural History Bulletin, art. 3, v. 158, p. 263-371.

Smithson, S.B., and Hodge, D.S., 1972, Field relations and gravity interpretations in the Laramie anorthosite complex: Wyoming Univ. Contr. Geology, v. 11 p. 43-59.

Stanley, K.O., 1971, Tectonic implications of Tertiary sediment dispersal on the Great Plains east of the Laramie Range: Wyoming Geol. Assoc. Guidebook 23d Ann. Field Conf., p. 65-70.

Stanley, K.O, 1976, sandstone petrofacies in the Cenozoic High Plains sequence, eastern Wyoming and Nebraska: Geological Society of America Bulletin, v. 87, p. 297-309.

Stanley, K.O., and Benson, L.V., 1979, Early diagenesis of High Plains Tertiary vitric and arkosic sandstone, Wyoming and Nebraska: SEPM Special Publication, No. 26, p. 401-423.

Swinehart, J.B., 1981, Plio-Pleistocene inner channel deposits in a bedrock incised valley, western Nebraska: Geological Society of America, Abstracts with Programs, v. 13, p. 227.

Swinehart, J.B., Souders, V.L., DeGraw, H.M., and Diffendal, Jr., R.F., 1985, Cenozoic paleogeography of western Nebraska, *in* Flores, R.M., and Kaplan, editors, Cenozoic paleogeography of West-Central United States: Raocy Mountain section-Society of Economic Paleontologists and Mineralogists, p. 209-229.

Tallman, S.L., 1949, Sandstone types: their abundance and cementing agents: Jour. Geology: v. 57, p. 582-591.

Taylor, J.M., 1970, Pore-space reduction in sandstone: Am. Assoc. Petroleum Geologists Bull., v. 34, p. 701-716.

Todd, J.E., 1903, Concretions and their geological effects: Geological Society of America Bulletin, v. 14, p. 353-368.

Theakstone, W.H., 1981, Concretions in glacial sediments at Seglavatnet, Norway: Journal of Sedimentary Petrology, v. 51, p. 191-196.

Vicars, R.G., and Breyer, J.A., 1981, Sedimentary facies in air-fall pyroclastic debris, Arikaree Group (Miocene), northwest Nebraska, U.S.A.: Journal of Sedimentary Petrology, v. 51, p. 900-921.

Walker, T.R., 1967, Formation of red beds in modern and ancient deserts: Geol. Soc. America Bull., v. 78, p. 353-368.

Walker, T.R., 1976, Diagenetic origin of continental red beds, in H. Galke (ed.), The continental Permian in central, west, and south Europe: Dordrecht, Holland, D. Reidel Pub. Co., p. 240-282.

Wanless, H.R., 1922, Notes on sand calcite from South Dakota: American Mineralogist, v. 11, No. 2, p. 83-86.

Wanless, H.R., 1922, Lithology of the White River sediment: Am. Philos. Soc. Proc., v. 61, p. 184-203.

Wanless, H.R., 1923,j The stratigraphy of the White River beds of South Dakota: Am. Philos. Soc. Proc., v. 62, p. 190-269.

Wilkinson, Mark., 1991, The concretions of the Bearreraig Sandstone Formation: geometry and geochemistry; Sedimentology, v. 38, p. 899-912.

Wilkinson, Mark, and M.D. Dampier, 1990, The rate of growth of sandstone-hosted calcite concretions: Geochimica et Cosmochimica Acta, v. 54, p. 3391-3399.

Wilson, M.D., and Pittman, 1977, Authigenic clays in sandstone: recognition and influence on reservoir properties and paleoenvironmental analysis: Journal of Sedimentary Petrology, v. 47, No. 1, p. 3-31.

The vita has been removed from the digitized version of this document.